

previous evaluation working with Eq. (64) in analogy with the Casimir technique.

In the published literature, there is some disagreement on the evaluation of the temperature dependence of retarded dispersion forces, the results of Lifshitz being in disagreement with the results of Sauer which are further supported by our work here. It has been suggested by a number of authors¹⁶ that Lifshitz's calculations are probably in error in this case.

¹⁶ C. M. Hargreaves, Koninkl. Ned Akad. Wetenschap, Proc. **B68**, 231, (1965). See also Sauer in Ref. 15. The present author has carried out numerical calculations of the Helmholtz free energy of a partition for a conducting parallelepiped (to be published).

IV. CONCLUSIONS

In summary then, the theory of the free quantum electromagnetic field may be regarded as a convenient description of a classical electromagnetic field subject to stochastic random fluctuations. Hence, it is easy to understand the connection between the various calculations for retarded dispersion forces between metals. Starting from the situation of a classical fluctuating field, the analysis as given by Lifshitz merely takes a different route from that leading to the quantum mechanical description which was used as a starting point by Casimir.

pp Interactions at 10 GeV/c

S. P. ALMEIDA,* J. G. RUSHBROOKE, AND J. H. SCHARENGUIVEL†
Cavendish Laboratory, Cambridge, England

AND

M. BEHRENS, V. BLOBEL, I. BORECKA, H. C. DEHNE,‡ J. DÍAZ,§ G. KNIES, A. SCHMITT,
 K. STRÖMER, AND W. P. SWANSON||

Deutsches Elektronen-Synchrotron DESY, Hamburg, Germany
 and

Physikalisches Staatsinstitut, II. Institut für Experimentalphysik der Universität Hamburg, Germany

(Received 12 April 1968)

About 3700 two-prong and 5600 four-prong events of 10-GeV/c pp interactions in the Saclay 81-cm hydrogen bubble chamber have been measured and analyzed. The reliability of the identification of the different final states has been checked using Monte Carlo-generated events. For the channels accessible to analysis, cross sections and invariant-mass distributions are given. The c.m. angular distributions and the mean values of the transverse momentum for all final-state particles are shown and discussed. Production of $\Delta^{++}(1236)$ accounts for about 30% of the cross section $\sigma(pp \rightarrow pn\pi^+) = 4.1 \pm 0.4$ mb. About 50% of the cross section $\sigma(pp \rightarrow pp\pi^+\pi^-) = 2.4 \pm 0.2$ mb can be accounted for by Δ^{++} production. Production of nucleon isobars at 1450, 1520, and 1730 MeV and their subsequent decay into $p\pi^+\pi^-$ are investigated. Their cross sections, t dependences, and branching ratios are determined, using a one-pion-exchange model (OPEM) for calculating the background distributions. The production of resonances decaying into $p\pi^-$ at 1236, 1500, and 1690 MeV is seen, and cross sections are given. Resonance production in the $pp\pi^+\pi^-\pi^0$ and $pn\pi^+\pi^+\pi^-$ reactions is studied using background curves calculated with a model based on simple parametrizations of the c.m. momentum distributions. The production of nucleon isobars accounts for nearly 100% of these reactions. For the reactions $pp \rightarrow pp\omega$, $pp\eta$, and ppf^0 , the cross sections found are 0.16 ± 0.03 , 0.16 ± 0.07 , and 0.10 ± 0.04 mb, respectively, corrected for unobserved decay modes. It is shown that most of the gross features of the pion-production reactions can be explained by the OPEM with the form factors of Ferrari and Selleri.

1. INTRODUCTION

PROTON-PROTON interactions at high energies have been studied by a number of groups, using bubble chambers¹⁻⁵ or counters.⁶⁻⁹ The salient features

* Present address: Virginia Polytechnic Institute, Blacksburg, Va.

† Present address: Harvard University, Cambridge, Mass.

‡ Present address: Laboratori Nazionali di Frascati del C.N.E.N. Frascati, Italy.

§ Present address: CERN, TC Division, Geneva, Switzerland.

|| Fellow of the Stiftung Volkswagenwerk. Present address: Stanford University, Stanford, Calif.

¹ A list of references for previous work at lower energy can be found, for example, in G. Alexander, O. Benary, G. Czapek, B.

seen in these reactions are strong $\Delta(1236)$ isobar production and the production of several of the $T = \frac{1}{2}$ isobar states having both elastic and inelastic decay modes.

Haber, N. Kidron, B. Reuter, A. Shapira, E. Simonopoulou, and G. Yekutieli, Phys. Rev. **154**, 1284 (1967). Subsequent publications are Refs. 2-5.

² Two-prong events at 4.0 GeV/c: S. Coletti, J. Kidd, L. Mandelli, V. Pelosi, S. Ratti, V. Russo, L. Tallone, E. Zampieri, C. Caso, F. Conte, M. Dameri, C. Grosso, and G. Tomasini, Nuovo Cimento **49A**, 479 (1967).

³ Four-prong events at 5.0 GeV/c: A. P. Colleraine and U. Nauenberg, Phys. Rev. **161**, 1387 (1967); A. P. Colleraine, Princeton Pennsylvania Accelerator Report No. PPAD-600F, 1966 (unpublished).

⁴ There are several bubble-chamber investigations of high-

Of the boson resonances η and ω have been observed. In all reactions the final-state nucleons appear highly collimated forward and backward with respect to the beam direction, indicating pronounced peripherality.

In this paper, we present results on proton-proton interactions at 10 GeV/c with two and four secondary tracks without visible strange-particle decays. Some results on the reaction $p\bar{p} \rightarrow p\bar{n}\pi^+$ and on the production of the $N^*(1450)$ isobar have already been published.^{10,11}

The six-prong events and strange particles have been studied at the University of Stockholm.¹²

The paper is organized into the following sections:

1. Introduction
 2. Experimental Procedure
 3. Cross Sections
 4. Angular and Momentum Distributions
 5. Elastic Scattering
 6. Reaction $p\bar{p} \rightarrow p\bar{n}\pi^+$
 7. Reaction $p\bar{p} \rightarrow p\bar{p}\pi^+\pi^-$
 - A. Reaction $p\bar{p} \rightarrow \Delta^{++}p\pi^-$
 - B. Reaction $p\bar{p} \rightarrow p\bar{N}^{*+} \rightarrow p(p\pi^+\pi^-)$
 1. Selection of the Resonant Combinations
 2. Analysis of $p\pi^+\pi^-$ Resonances
 3. Decay of $N^*(p\pi^+\pi^-)$ Resonances
 - C. Resonances in $p\pi^-$
 - D. Resonances in $\pi^+\pi^-$
 - E. Comparison with the OPEM
 1. Qualitative Evidence for OPEM
 2. Check of the Double-Isobar Diagram
 8. Reaction $p\bar{p} \rightarrow p\bar{p}\pi^+\pi^0$
 9. Reaction $p\bar{p} \rightarrow p\bar{n}\pi^+\pi^+\pi^-$
 10. Conclusions
- Appendices:
- A. Monte Carlo Estimate of the Contamination Matrices
 - B. Evaluation of the OPEM with Ferrari-Selleri Form Factors

energy $p\bar{p}$ interactions without strange-particle production in progress: (a) Four-prong events at 4.0 and 6.0 eGV/c: C. Caso, M. Dameri, S. Ratti, E. Russo, E. Zampieri, I. Bloodworth, L. Lyons, and A. Norton, in *Proceedings of the Thirteenth Annual International Conference on High-Energy Physics, Berkeley, 1966* (University of California Press, Berkeley, 1967); C. Caso, F. Conte, G. Tomasini, L. Casè, L. Mosca, L. Tallone-Lombardi, S. Ratti, I. Bloodworth, L. Lyons, and A. Norton, *Nuovo Cimento* **55A**, 66 (1968). (b) Two-prong events at 6.0 GeV/c: C. Caso, G. Tomasini, L. Mosca, S. Ratti, I. Bloodworth, L. Lyons, and A. Norton, in *Proceedings of the Thirteenth Annual International Conference on High-Energy Physics, Berkeley, 1966* (University of California Press, Berkeley, 1967). (c) Four-prong events at 6.0 GeV/c: W. Chinowsky, P. Condon, R. R. Kinsey, S. Klein, M. Mandelkern, P. Schmidt, J. Schultz, F. Martin, M. L. Perl, and T. H. Tan, *Phys. Rev.* **171**, 1421 (1968); T. H. Fan, F. Martin, M. Perl, W. Chinowsky, R. Kinsey, S. Klein, M. Mandelkern, and J. Schultz, *Bull. Am. Phys. Soc.* **12**, 10 (1967). (d) Four-prong events at 8 GeV/c: D. Grether, G. Ascoli, M. Firebaugh, E. L. Goldwasser, R. D. Sard, and J. Wray, *ibid.* **12**, 10 (1967). (e) Four-prong events at 16 GeV/c: Cambridge-London (I.C.) Collaboration (unpublished); J. R. Williams (private communication); (f) Four-prong events at 22 GeV/c: W. J. Kernan, Jr., Y. W. Kang, R. A. Leacock, J. I. Rhode, T. L. Schalk, and L. S. Schroeder, *Bull. Am. Phys. Soc.* **12**, 488 (1967); L. S. Schroeder, in *Proceedings of the 1967 Boulder Conference on High-Energy Physics* (unpublished); and (private communication). (g) Six-prong events at 28 GeV/c: P. L. Connolly, I. R. Kenyon, D. J. Miller, T. W. Morris, R. S. Panvini, D. C. Rahm, C. R. Richardson, and A. M. Thorndike, *Bull. Am. Phys. Soc.* **12**, 488 (1967). (h) Two- and four-prong events at 28 GeV/c: P. L. Connolly, E. L. Hart, T. W. Morris, R. Panvini, D. C. Rahm, C. R. Richardson, and A. M. Thorndike, Brookhaven National Laboratory Report No. BNL-10573, 1966 (unpublished).

⁵ At the Heidelberg International Conference on Elementary Particles, 1967, the following contributions were submitted on bubble-chamber investigations of $p\bar{p}$ interactions at high energies:

2. EXPERIMENTAL PROCEDURE

The experiment has been carried out with pictures taken in the 81-cm Saclay hydrogen bubble chamber, exposed to a 10.01 ± 0.01 -GeV/c proton beam¹³ at the CERN proton synchrotron. The average flux was 10.2 ± 0.1 protons per picture.

Approximately 80 000 pictures (about 30 000 for the two-prong events) were scanned. The average ionization density was 14 bubbles/cm for a minimum-ionizing track.

The beam contamination in the bubble chamber was determined by three independent methods: (a) determination of the physical separation of the p and π^+ components in the beam using counter methods, (b) a Čerenkov counter in the beam, and (c) fitting the spectra of δ rays with momenta higher than 50 MeV/c produced by beam tracks. The total ($\pi^+ + \mu^+ + e^+$) contamination was determined to be less than 1%.

A fiducial region 26 cm long (13 cm in half of the sample) was chosen so as to assure a minimum track length of 30 cm for secondary tracks going in the for-

(a) Two-prong events at 6.92 GeV/c: G. Alexander, Z. Carmel, Y. Eisenberg, E. Ronant, A. Shapira, G. Yekutieli, A. Fridman, G. Maurer, J. Oudet, C. Zech, and P. Cüer, Rehovoth-Strasbourg Collaboration, in *Proceedings of the Heidelberg International Conference on Elementary Particles*, edited by H. Filthuth (Interscience Publishers, Inc., New York, 1968), p. 522; (b) Four-prong events at 8.1 GeV/c: J. le Guyader, G. Kayas, M. Sene, T. P. Yiou, J. Ginestet, D. Manesse, Tran Ha Anh, J. Alitti, Nguyen Thuc Diem, and G. Smadja, Orsay-Saclay Collaboration, *ibid.* p. 521; (c) Four-prong events at 19 GeV/c: Copenhagen-Helsinki-Oslo-Stockholm Collaboration, *ibid.* p. 527. At the American Physical Society Meeting in Washington, 1968, the following contributions on high-energy $p\bar{p}$ bubble-chamber investigations were submitted: (d) R. Ehrlicher, R. Nieperont, R. Plano, J. B. Whittacker, C. Baltay, J. Feinman, P. Franzini, R. Newman, and N. Yeh, *Bull. Am. Phys. Soc.* **13**, 682 (1968). (e) W. E. Ellis, P. L. Connolly, J. D. Miller, T. W. Morris, and R. S. Panvini, *ibid.* **13**, 682 (1968).

⁶ E. W. Anderson, E. J. Bleser, G. B. Collins, T. Fujii, J. Menes, F. Turkot, R. A. Carrigan, Jr., R. M. Edelman, N. C. Hien, T. J. McMahon, and I. Nadelhaft, *Phys. Rev. Letters* **16**, 855 (1966); a detailed list of references on missing-mass $p\bar{p}$ experiments is given, for example, in I. M. Blair, A. E. Taylor, W. S. Chapman, P. I. P. Kalmus, J. Litt, M. C. Miller, D. B. Scott, H. J. Sherman, A. Astbury, and T. G. Walker, *ibid.* **17**, 789 (1966). Subsequent publications are Refs 7-9.

⁷ H. L. Anderson, S. Fukui, D. Kessler, K. A. Klare, M. V. Sherbrook, H. J. Evans, R. L. Martin, E. P. Hincks, N. K. Sherman, and P. I. P. Kalmus, *Phys. Rev. Letters* **18**, 89 (1967).

⁸ K. J. Foley, R. S. Jones, S. J. Lindenbaum, W. A. Love, S. Ozaki, E. D. Platner, C. A. Quarles, and E. H. Willen, *Phys. Rev. Letters* **19**, 397 (1967).

⁹ E. W. Anderson, E. J. Bleser, G. B. Collins, T. Fujii, J. Menes, F. Turkot, R. A. Carrigan, Jr., R. M. Edelman, N. C. Hien, T. J. McMahon, and I. Nadelhaft, *Phys. Rev. Letters* **19**, 198 (1967); E. W. Anderson and G. B. Collins, *ibid.* **19**, 201 (1967).

¹⁰ H.-C. Dehne, J. Diàz, K. Strömer, A. Schmitt, W. P. Swanson, I. Borecka, G. Knies, and G. Wolf, *Nuovo Cimento* **53A**, 232 (1968).

¹¹ S. P. Almeida, J. G. Rushbrooke, J. H. Scharenguiel, M. Behrens, V. Blobel, H. C. Dehne, J. Diàz, R. Schäfer, W. P. Swanson, I. Borecka, and G. Knies, *Nuovo Cimento* **50A**, 1000 (1967).

¹² S. O. Holmgren, S. Nilsson, T. Olhede, and N. Yamdagni, *Nuovo Cimento* **57A**, 20 (1968); S. O. Holmgren, S. Nilsson, T. Olhede, and N. Yamdagni, *ibid.* **51A**, 305 (1967).

¹³ E. Keil and W. W. Neale, CERN Report No. TC/02, 1962 (unpublished).

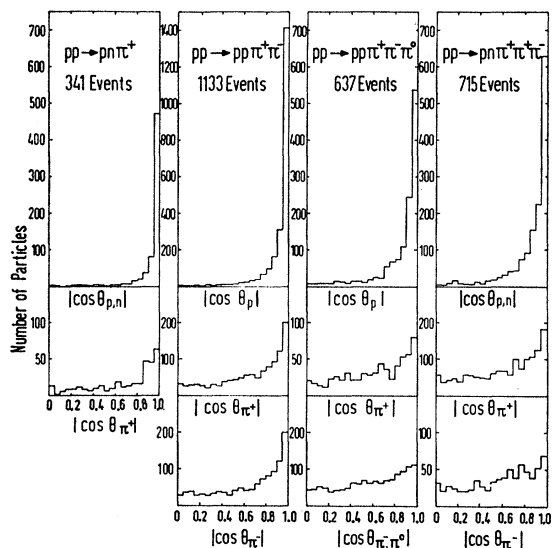


FIG. 1. Distributions of the cosine of the particle production angle θ , folded around 90° , for reactions (3)–(6). The symbol $\theta_{p,n}$ means the c.m. angle of proton or neutron with respect to the beam direction.

ward direction and a minimum track length of 10 cm for the primary proton. The film was scanned twice.

The two-prong events and part of the four-prong events were measured at Hamburg and processed using the geometrical reconstruction program WELAGA and the CERN kinematical program GRIND. The other four-prong events were measured at the Cavendish laboratory and processed by the fitting program TONY.¹⁴ All other kinematical calculations and plots were made using the program HYBRID-ULTRAN.¹⁵ In addition to the kinematical fitting, particles were identified up to a momentum of 1.7 GeV/c by mean-gap-length measurements.

Approximately 3700 two-prong and 5600 four-prong events were measured. About 3% could not be analyzed because of measuring difficulties, the main contribution coming from events with a secondary interaction near the vertex.

An event was taken to fit a given hypothesis if its χ^2 value was less than 6 for a one-constraint (one-C) fit or 15 for a four-constraint (four-C) fit.

Events were attributed to a hypothesis with more than one neutral particle (no-fit) if the missing four-momentum for that hypothesis was consistent with the presence of more than one neutral particle in the final state. Details of assignment of hypotheses are given in Secs. 6, 8, and 9.

In order to check the measuring and identification procedure from the Cambridge and Hamburg groups, a

¹⁴ J. Zoll, Ph.D. thesis, Cambridge University, 1961 (unpublished); B. A. Westwood, Ph.D. thesis, Cambridge University, 1964 (unpublished).

¹⁵ H. Butenschön, DESY Report No. 66/29, 1966 (unpublished), and private communication.

TABLE I. Topological cross sections in mb.

| Two-prong | Four-prong | Six-prong | Eight-prong | Total |
|----------------|----------------|-----------------|-----------------|----------------|
| 24.7 ± 1.1 | 12.7 ± 0.6 | 2.40 ± 0.15 | 0.22 ± 0.04 | 41.1 ± 1.7 |

sample of 20 events were processed at both laboratories and compared. The results were in good agreement.

3. CROSS SECTIONS

For the total interaction cross section a value of $\sigma_{\text{tot}} = 41.1 \pm 1.7$ mb was obtained based on the track length scanned and the number of events found in 18 rolls and assuming a hydrogen density of 0.0625 g/cm³. The values of $\sigma_{\text{tot}} = 39.9 \pm 0.6$,¹⁶ 40.2 ± 0.3 ,¹⁷ and 39.84 ± 0.12 mb¹⁸ from counter experiments are in agreement with our results. Corrections have been made for scanning losses, beam attenuation within the fiducial volume, and beam contamination. A correction of 2.1 mb for systematic loss of small-angle pp elastic scattering events has also been applied (see Sec. 5).

The topological cross sections, corrected as above, are given in Table I. The partial cross sections do not include visible decays of strange particles.

Owing to the high momentum of the incoming particle, the symmetry of pp interactions, and the peripherality of the reaction, protons and π^+ mesons both occur frequently in the final state with laboratory momenta larger than 1.7 GeV/c. Therefore ambiguities among one-C and no-fit hypotheses are very numerous. The ambiguities have been studied with two different methods.

TABLE II. Cross sections in mb.

| Channel | Corrected cross section |
|--|-------------------------|
| (1) pp | 10.2 ± 0.6 |
| (2) $pp\pi^0$ | 1.4 ± 0.3 |
| (3) $pn\pi^+$ | 4.1 ± 0.4 |
| (4) $pp\pi^+\pi^-$ | 2.4 ± 0.2 |
| (5) $pp\pi^+\pi^-\pi^0$ | 2.3 ± 0.2 |
| (6) $pn\pi^+\pi^-\pi^0$ | 2.4 ± 0.2 |
| $pp(m\pi^0)$, $m \geq 2$ | ~ 1.5 |
| $pn\pi^+(m\pi^0)$, $m \geq 1$ | ~ 5.3 |
| $nn\pi^+\pi^+(m\pi^0)$, $m \geq 0$ | ~ 2.2 |
| $pp\pi^+\pi^-(m\pi^0)$, $m \geq 2$ | ~ 0.7 |
| $pn\pi^+\pi^-\pi^-(m\pi^0)$, $m \geq 1$ | ~ 4.1 |
| $nn\pi^+\pi^+\pi^-(m\pi^0)$, $m \geq 0$ | ~ 0.8 |

¹⁶ W. Galbraith, E. W. Jenkins, T. F. Kycia, B. A. Leontic, R. H. Phillips, A. L. Read, and R. Rubinstein, Phys. Rev. **138**, B913 (1965).

¹⁷ G. Bellettini, G. Cocconi, A. N. Diddens, E. Lillethun, J. Pahl, J. P. Scanlon, J. Walthers, A. M. Wetherell, and P. Zanella, Phys. Letters **14**, 164 (1965); G. Bellettini, G. Cocconi, A. N. Diddens, E. Lillethun, J. P. Scanlon, and A. M. Wetherell, *ibid.* **19**, 705 (1966).

¹⁸ K. J. Foley, R. S. Jones, S. J. Lindenbaum, W. A. Love, S. Ozaki, E. D. Plattner, C. A. Quarles, and E. H. Willen, Phys. Rev. Letters **19**, 857 (1967).

In method I, Monte Carlo events were generated with the program FAKE¹⁹ for the most copious channels and processed in the same way as the real events. Contamination matrices were determined and used to calculate various cross sections. The contamination matrices give the sources of ambiguity in compact form. A description of the method is given in Appendix A.

In method II, we examined the apparent deviations from symmetry about 90° in the c.m. system, in the distributions of production angles of particles and combinations of particles, caused by the ambiguous events. Criteria were established for each channel in order to select a reasonably pure sample. Details are given in the sections corresponding to each channel.

The samples of events resulting from method II were used in the subsequent analyses of reactions (3), (5), and (6) (Secs. 6, 8, and 9, respectively).

The values of the partial cross sections found with both methods agree within errors. The values given in Table II for the fitted channels represent a compromise (a mean value weighted with the errors of the corresponding method) between the two values. The errors on cross sections shown reflect the uncertainties inherent in the two methods used as well as the usual statistical errors. For the no-fit channels we have used only method I to determine cross sections. The corresponding errors are mainly due to uncertainties in the contamination matrix for channels with more than two neutral particles, and are estimated to be about 0.5 mb.

4. ANGULAR AND MOMENTUM DISTRIBUTIONS

Figure 1 shows the c.m. angular distributions, folded around 90°, for the various particles in reactions (3)–(6) listed in Table II.

TABLE III. Mean values $\langle p_t \rangle$ of transverse momenta and standard deviations σ_t and σ_l for transverse and longitudinal momenta, respectively.

| Reaction | Particle | $\langle p_t \rangle$ (MeV/c) | σ_t (MeV/c) | σ_l (MeV/c) |
|----------|----------|----------------------------------|-----------------------|-----------------------|
| (3) | Nucleon | 404±9 | 349±7 | |
| | π^+ | 384±11 | 329±9 | 658±25 |
| (4) | Nucleon | 390±5 | 327±4 | |
| | π^+ | 268±5 | 233±4 | 448±9 |
| | π^- | 337±5 | 284±4 | 533±11 |
| (5) | Nucleon | 422±6 | 345±5 | |
| | π^+ | 302±6 | 258±5 | 404±11 |
| | π^- | 332±6 | 275±5 | 379±11 |
| | π^0 | 345±7 | 288±6 | 392±11 |
| (6) | Nucleon | 435±6 | 359±5 | |
| | π^- | 312±5 | 264±4 | 424±8 |
| | π^+ | 296±6 | 247±5 | 356±9 |

¹⁹ G. R. Lynch, University of California Lawrence Radiation Laboratory Report No. UCRL-10335, 1962 (unpublished); E. Raubold, FAKE Manual, Hamburg, 1966 (unpublished). The Raubold version of FAKE contains modifications in the method of error handling.

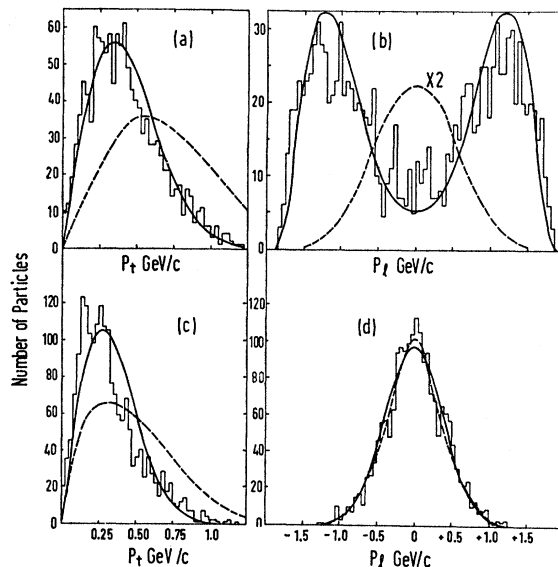


FIG. 2. Distribution of the transverse and longitudinal momenta p_t and p_l in the c.m. system: (a) and (b) for the protons and (c) and (d) for the pions for the reaction $p\bar{p} \rightarrow p\bar{p}\pi^+\pi^-\pi^0$. The dashed curves are predictions of Lorentz-invariant phase space. The full curves in (a), (c), and (d) are the fits described in the text. The full curve in (b) is calculated with the Monte Carlo program discussed in the text.

The forward-backward peaking of the nucleons along the incident-particle direction suggests that peripheral mechanisms are important in these reactions. The peaking of the nucleon c.m. angular distributions at $|\cos\theta| \simeq 1$ decreases with increasing number of pions in the final state.

The pion c.m. angular distributions are not so strongly peaked and also become flatter with increasing number of pions.

The transverse momenta of all particles are rather small compared with the nucleon longitudinal momenta.²⁰ The c.m. longitudinal-momentum distribution of the nucleons has a maximum in the forward and backward direction, while the longitudinal momenta of the pions are distributed in a small interval around zero. For example, see Fig. 2 for the distributions from reaction (5).

The momentum and angular distributions do not agree with Lorentz-invariant phase-space predictions [dashed curves in Figs. 2(a)–2(d)].

The mean transverse momenta $\langle p_t \rangle$ for particles from reactions (3)–(6) are given in Table III. The distributions of transverse momenta of all particles were fitted to the function

$$f(p_t)dp_t = (p_t/\sigma_t^2)\exp(-p_t^2/2\sigma_t^2) dp_t.$$

²⁰ For a complete set of two-dimensional plots, containing p_t versus p_l , see V. Blobel, Ph.D. thesis, Hamburg University (unpublished).

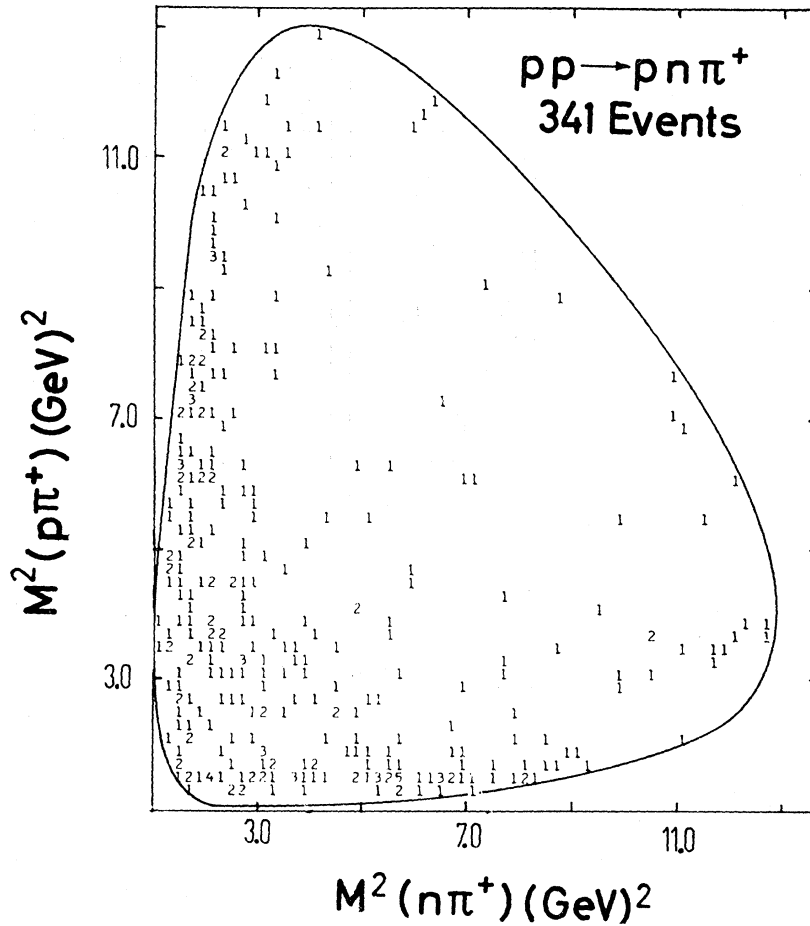


FIG. 3. Dalitz plot, $M^2(p\pi^+)$ versus $M^2(n\pi^+)$, for the final state $pn\pi^+$.

This function has been used by other authors^{21,22} and is consistent with a model having the two spatial components p_x and p_y of the transverse momentum $p_t = (p_x^2 + p_y^2)^{1/2}$ uncorrelated and normally distributed with zero mean and standard deviation σ_t .²² It is the simplest model that gives a reasonable description of the experimental distributions. The distributions of transverse momentum of the nucleons are well described by this function. The trend of the pion transverse-momentum distribution is also reproduced by this function, but there is a consistent deviation at high values of p_t . As an example, these fits for reaction (5) are shown in Figs. 2(a) and 2(c). The distribution of the longitudinal momentum $p_l = p_z$ of the pions is well described by a normal distribution with zero mean and standard

deviation σ_l . The fit for reaction (5) is shown in Fig. 2(d). The fitted parameters σ_t and σ_l are given in Table III for reactions (3)–(6).

The pion final-state momentum may thus be roughly characterized by normal distributions for p_x , p_y , and p_z , with standard deviations σ_t , σ_t , and σ_l , respectively. Use of this observation was made in calculating the longitudinal-momentum distributions of the nucleons and invariant-mass distributions for reactions (5) and (6). A Monte Carlo program was used to generate events by choosing normally distributed components of the transverse momentum of all particles and normally distributed longitudinal momenta of the pions in the c.m. system. Energy and momentum conservation then determined the longitudinal components of the nucleons. The distributions calculated from these randomly generated events indeed agree with the experimentally observed nucleon longitudinal-momentum distributions [see, for example, Fig. 2(b)], and provide useful background curves for the invariant-mass distributions (see Secs. 8 and 9).²³

²¹ K. Pinkau, *Phil. Mag.* **6**, 657 (1961).

²² E. M. Friedlander, *Nuovo Cimento* **41A**, 417 (1966), and references given therein; L. G. Ratner, K. W. Edwards, C. W. Akerlof, D. G. Crabb, J. L. Day, A. D. Krisch, and M. T. Lin [*Phys. Rev. Letters* **18**, 1218 (1967)] have made very precise measurements of the transverse- and longitudinal-momentum spectra of various particles in 12.5-GeV/c $p\bar{p}$ collisions; G. Drews [*Diplomarbeit*, Hamburg University, 1967 (unpublished)] has shown that for π^-p interactions at 11 GeV/c simple models (such as the one used here) are a bad approximation, owing to strong effects of the meson resonances.

²³ This method arose from discussion with G. Drews and H. Nagel, who make a similar calculation for π^-p interactions, also based on transverse-momentum distributions.

5. ELASTIC SCATTERING

The numbers of events found at different intervals of the four-momentum transfer $t(p_{\text{in}}, p_{\text{out}})$ were corrected for beam contamination, scanning losses, unmeasurable events, and systematic losses at small angles.²⁴ An additional uncertainty of $\pm 7\%$, due to the calculated value of the correction for systematic and scanning losses, was added.

The differential cross section $d\sigma/d|t|$ was fitted to the function

$$d\sigma/d|t| = \exp(a - b|t| + ct^2),$$

using the experimental points in the interval $0.015 \leq |t| \leq 0.510$ (GeV/c)². The values found for the parameters, and therefore the total elastic cross section $\sigma_{\text{el}} = 10.2 \pm 0.9$ mb, agree within the error limits with the precise measurements of Foley *et al.*,²⁵ $\sigma = 11.04 \pm 0.22$ mb at 10.8 GeV/c. These and other authors have made measurements of elastic scattering, at various values of momentum transfer.^{17, 18, 26-28}

6. REACTION $p\bar{p} \rightarrow p\bar{n}\pi^+$

For this reaction, events having the π^+ in the backward hemisphere in the c.m. system relative to the incident proton direction are $(90 \pm 5)\%$ correctly identified,¹⁰ and only these events have been used for the analysis (341 events). We have checked with FAKE¹⁹-generated events that resonancelike contaminations to the mass distributions from resonances of final states with additional π^0 's are less than $40 \mu\text{b}$. This number is much smaller than the statistical errors in Table IV. The main contribution to the contamination comes from the final state $p\bar{p}\pi^0$.

In Fig. 3 the Dalitz plot for the final state, $M^2(p\bar{p}\pi^+)$ versus $M^2(n\pi^+)$, is shown,²⁹ and in Fig. 4 the invariant-mass histograms are given. The curves show the pre-

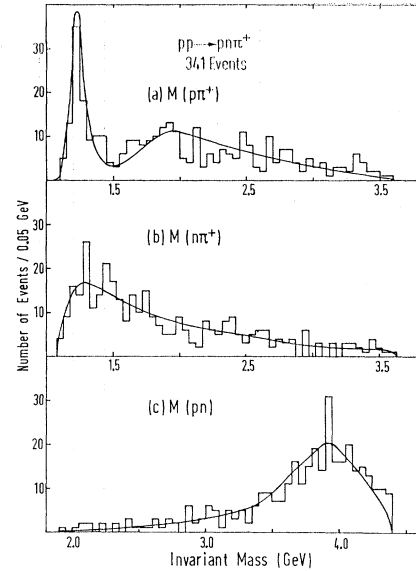


FIG. 4. Invariant-mass distributions for the reaction $p\bar{p} \rightarrow p\bar{n}\pi^+$. (a) $p\bar{p}\pi^+$; (b) $n\pi^+$; (c) $p\bar{n}$. The curves are calculated according to the OPEM and normalized to the number of events.

dictions of the one-pion-exchange model (OPEM) with form factors from Ferrari and Selleri ($\gamma = 15m_\pi^2$), calculated using diagram 1 of Appendix B, Fig. 22, normalized to the number of events.

The $\Delta^{++}(1236)$ is clearly seen in the $p\bar{p}\pi^+$ mass distribution. The enhancements at 1900 MeV in $p\bar{p}\pi^+$ and at 1450 MeV in $n\pi^+$ have been discussed in Refs. 10 and 11, respectively. The cross sections for resonance production in this channel are given in Table IV. A comparison of the $\Delta^{++}(1236)$ production with several OPE calculations was also made in Ref. 10. At our energy there is little contamination from other channels and the background due to diagram 2 of Appendix B is estimated to be less than 10%. Therefore this reaction is especially well suited for an analysis of the type suggested by Gellert *et al.*³⁰ This analysis compares the shape parameters of the π^+p -decay angular distribution for the nucleon-pion vertex of diagram 1 (Appendix B) with the shape parameters of free π^+p scattering.

We have calculated the mean values of the Y_l^m obtained from the experimental distributions by averaging

TABLE IV. Partial cross sections in mb for reaction $p\bar{p} \rightarrow p\bar{n}\pi^+$.

| Reaction | Cross section ^a |
|---|----------------------------|
| $p\bar{p} \rightarrow \Delta^{++}(1236)n$ | 1.18 ± 0.14 |
| $p\bar{p} \rightarrow \Delta^{++}(1920)n$ | 0.38 ± 0.11 |
| $p\bar{p} \rightarrow N^{*+}(1450)p$ | 0.20 ± 0.13 |

^a Cross sections given in the table refer only to those decays of the resonances involved, which lead to the final state $p\bar{n}\pi^+$.

³⁰ E. Gellert, G. A. Smith, S. Wojcicki, E. Colton, P. E. Schlein, and H. K. Ticho, Phys. Rev. Letters **17**, 884 (1966).

²⁴ K. Böckmann, B. Nellen, E. Paul, B. Wagini, I. Borecka, J. Diáz, U. Heeren, U. Liebermeister, E. Lohrmann, E. Raubold, P. Söding, S. Wolf, J. Kidd, L. Mandelli, L. Mosca, V. Pelosi, S. Ratti, and L. Tallone, Nuovo Cimento **42A**, 954 (1966).

²⁵ K. J. Foley, S. J. Lindenbaum, W. A. Love, S. Ozaki, J. J. Russell, and L. C. L. Yuan, Phys. Rev. Letters **11**, 425 (1963).

²⁶ K. J. Foley, R. S. Gilmore, S. J. Lindenbaum, W. A. Love, S. Ozaki, E. H. Willen, R. Yamada, and L. C. L. Yuan, Phys. Rev. Letters **15**, 45 (1965).

²⁷ D. Hartig, P. Blackall, B. Elsner, A. C. Helmholz, W. C. Middlekoop, B. Powell, B. Zacharov, P. Zanella, P. Dalpiaz, M. N. Focacci, S. Focardi, G. Giacomelli, L. Monari, J. A. Beaney, R. A. Donald, P. Mason, L. W. Jones, and D. O. Caldwell, Nuovo Cimento **38**, 60 (1965).

²⁸ (a) G. Cocconi, V. T. Cocconi, A. D. Krisch, J. Orear, R. Rubinstein, D. B. Scarf, B. T. Ulrich, W. F. Baker, E. W. Jenkins, and A. L. Read, Phys. Rev. **138**, B165 (1965); (b) C. W. Akerlof, R. H. Hieber, A. D. Krisch, K. W. Edwards, L. G. Ratner, and K. Ruddick, *ibid.* **159**, 1138 (1967); (c) J. V. Allaby, G. Cocconi, A. N. Diddens, A. Klovning, G. Matthiae, E. J. Sacharidis, and A. M. Wetherell, Phys. Letters **25B**, 156 (1967), and references given therein.

²⁹ In Fig. 3, as in the Figs. 7, 9, 10, 12, and 18, the format has been chosen to give more information than the usual two-dimensional plot with points. From these figures it is very simple to obtain histograms on one axis for different intervals on the other axis. More important, it is possible to make fits to the complete two-dimensional distributions. See, for example, Secs. 7 B and 7 C.

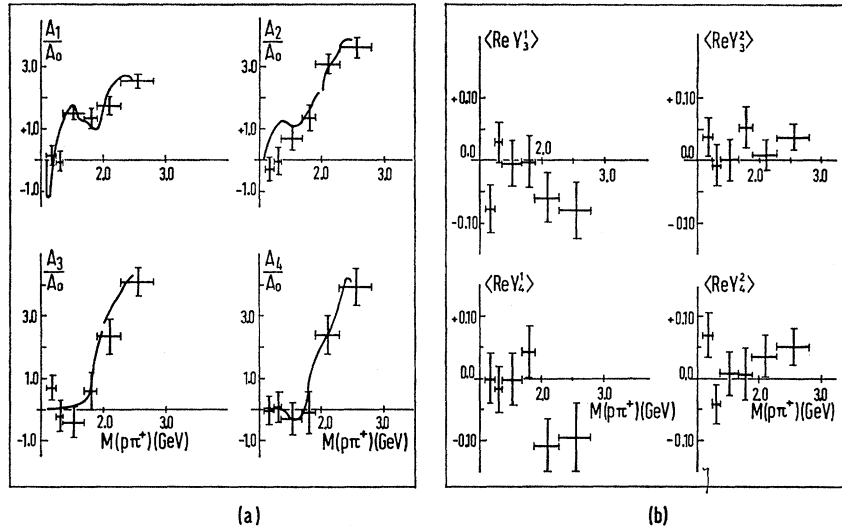


FIG. 5. Shape parameters for the $p\pi^+$ vertex of the reaction $p p \rightarrow p n \pi^+$ for events with small four-momentum transfer $t(p_{\text{in}}, p_{\text{out}}) \leq 0.3$ (GeV/c)². (a) The A_l/A_0 moments for $l \leq 4$. The smooth curves are the shape parameters derived from free $\pi^+ p$ elastic scattering. (b) The moments $\langle \text{Re} Y_3^1 \rangle$, $\langle \text{Re} Y_3^2 \rangle$, $\langle \text{Re} Y_4^1 \rangle$, and $\langle \text{Re} Y_4^2 \rangle$.

over the N events of a given $M(p\pi^+)$ interval:

$$\langle Y_l^m \rangle = \frac{1}{N} \sum_{i=1}^N Y_l^m(\cos\theta_i, \phi_i)$$

and

$$\Delta \langle Y_l^m \rangle = \frac{1}{N} [(\langle Y_l^m \rangle^2) - \langle Y_l^m \rangle^2]^{1/2},$$

where (as defined by Jackson³¹) the decay angle θ is the angle between incoming and outgoing proton in the $p\pi^+$ rest system and the azimuthal angle ϕ , defined in the same coordinate system, is zero for decay in the production plane, i.e.,

$$\cos\theta \equiv \frac{\mathbf{p}_1 \cdot \mathbf{p}}{|\mathbf{p}_1| |\mathbf{p}|}$$

and

$$\cos\phi \equiv \frac{\mathbf{p}_1 \times \mathbf{p} \cdot \mathbf{p}_2 \times \mathbf{n}}{|\mathbf{p}_1 \times \mathbf{p}| |\mathbf{p}_2 \times \mathbf{n}|}.$$

The \mathbf{p} vectors represent the momenta indicated in diagram 1 in Fig. 22.

The Y_l^m are defined as

$$Y_l^m(\cos\theta, \phi) = \left(\frac{2l+1}{4\pi} \frac{(l-m)!}{(l+m)!} \right)^{1/2} P_l^m(\cos\theta) e^{im\phi},$$

where $P_l^m(\cos\theta)$ are the associated Legendre polynomials. In terms of these Y_l^m the shape parameters defined by Gellert *et al.*³⁰ are

$$A_l/A_0 = [(2l+1)4\pi]^{1/2} \langle Y_l^0 \rangle.$$

Figure 5(a) shows the shape parameters A_l/A_0 as a function of $M(p\pi^+)$. The smooth curves are the shape parameters derived from free $\pi^+ p$ elastic scattering; the curves

were drawn through points calculated from the values given in Refs. 32(a)–32(c).

Parity conservation in the production processes requires $\langle \text{Im} Y_l^m \rangle = 0$. Our experimental values for $\langle \text{Im} Y_l^m \rangle$ are compatible with zero within statistics. In the OPEM with form factors but without absorption, $\langle \text{Re} Y_l^m \rangle$ must also be zero for all $m \neq 0$. Figure 5(b) gives the values of $\langle \text{Re} Y_l^m \rangle$ as a function of $M(p\pi^+)$ for $m \neq 0$ and $l \leq 4$. Only if $\langle \text{Re} Y_l^m \rangle$ deviates from zero with more than one standard deviation in at least three mass intervals are the values given. It can be seen in the figure that for various intervals some of them (see e.g., Y_3^1 , Y_4^1 , and Y_4^2) are incompatible with zero, which suggests that absorption and other processes are present.³³

7. REACTION $p p \rightarrow p p \pi^+ \pi^-$

According to our study of contamination in the various reactions (Sec. 2 and Appendix A), this reaction can be readily separated from other final states, and the sample used in the analyses described is believed to contain 99% correctly identified events. Figures 6–11 show the invariant-mass distributions of this reaction. There is a prominent $\Delta^{++}(1236)$ peak in the $p\pi^+$ distribution, indicating that a large fraction of the events proceed through $\Delta^{++} p \pi^-$. Two significant peaks are

³² (a) For $M(p\pi^+) < 1300$ MeV: L. D. Roper, R. M. Wright, and B. T. Field, *Phys. Rev.* **138**, B190 (1965); (b) For $1300 \leq M(p\pi^+) < 2020$ MeV: P. Bareyre, C. Bricman, and G. Villet *Phys. Rev.* **165**, 1730 (1968); (c) For $M(p\pi^+) \geq 2020$ MeV: E. H. Bellamy, T. F. Buckley, R. W. Dobinson, P. V. March, J. A. Strong, R. N. F. Walker, W. Busza, B. G. Duff, D. A. Garbutt, F. F. Heyman, C. C. Nimmon, K. M. Potter, and T. P. Swetman, *Phys. Rev. Letters* **19**, 476 (1967).

³³ For the $\Delta^{++}(1236)$ with $J^P = \frac{3}{2}^+$, $W(\cos\theta, \phi) = (4\pi)^{-1/2} \{ Y_0^0 + [(1-4\rho_{33})/5] Y_2^0 + (32/5)^{1/2} (\text{Re}\rho_{3,1} \text{Re}Y_2^1 - \text{Re}\rho_{3,-1} \text{Re}Y_2^2) \}$, where ρ_{ij} are the spin density-matrix elements as defined in Ref. 31. Making use of the orthogonality of the spherical harmonics, we can obtain the ρ_{ij} from the experimental $\langle Y_l^m \rangle$. For example, $\rho_{33} = \frac{1}{4} [1 - (\sqrt{20\pi}) \langle Y_2^0 \rangle] = \frac{1}{4} [1 - A_2/A_0]$. The values of all ρ_{ij} calculated in this way agree with the values obtained with the maximum-likelihood method discussed in Ref. 10.

³¹ J. D. Jackson, *Nuovo Cimento* **34**, 1644 (1964).

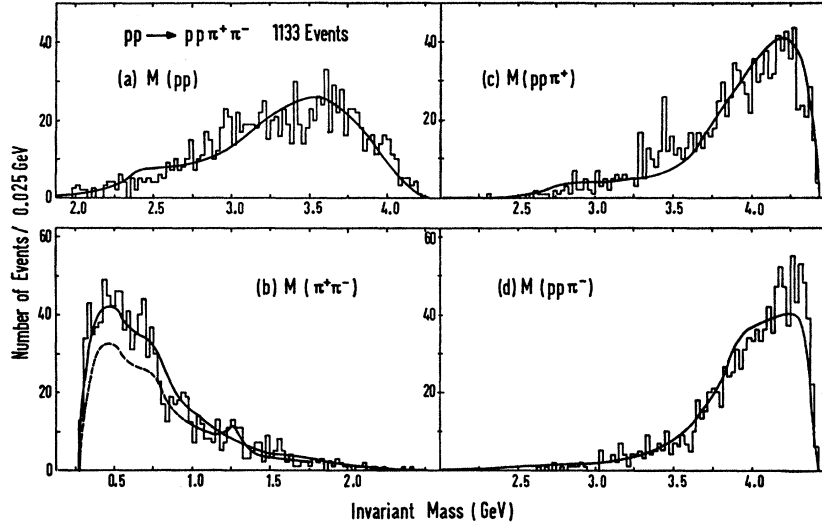


FIG. 6. Invariant mass distributions for the reaction $p\bar{p} \rightarrow p\bar{p}\pi^+\pi^-$. (a) $p\bar{p}$; (b) $\pi^+\pi^-$; (c) $p\bar{p}\pi^+$; (d) $p\bar{p}\pi^-$. The curves are calculated according to the OPEM and normalized to the number of events. The lower curve in (b) is from the f^0 fit described in Sec. 7 D.

present in the $p\pi^+\pi^-$ mass distribution at about 1.5 and 1.7 GeV. Indications of $\Delta^0(1236)$, $N^{*0}(1525)$, and $N^{*0}(1688)$ in the $p\pi^-$ mass distribution and of f^0 production in the $\pi^+\pi^-$ mass distribution are also present. No indications of resonances in the $p\bar{p}$ and $p\bar{p}\pi$ distributions are to be seen.

The curves shown in the figures are the predictions of the OPEM with Ferrari-Selleri form factors (see Appendix B), normalized to the number of events. They are in fair agreement with the histograms except for peaks in the $p\pi^+\pi^-$ distribution [Fig. 8(a)]. On the other hand, phase-space predictions (not shown) disagree violently with all distributions and are not suitable for describing the nonresonant background.

The main difficulties in the quantitative analysis of resonance production in this channel are (a) the ambiguities caused by the presence of two protons in the final state, (b) the influences of $p\pi^+\pi^-$ resonances on the $p\pi^+$ and $p\pi^-$ spectra and of the Δ^{++} resonance on the $p\pi^+\pi^-$ spectrum, and (c) the possible superposition of different resonances with similar masses in the $p\pi^+\pi^-$ spectrum. In order to overcome these difficulties, special methods for the analysis of the $p\pi^+$ and $p\pi^+\pi^-$ resonances were used.

A. Reaction $p\bar{p} \rightarrow \Delta^{++}p\pi^-$

The $p\pi^+$ mass distribution shows that a large fraction of reaction (4) proceeds through the reaction

$$p\bar{p} \rightarrow \Delta^{++}p\pi^-. \quad (4a)$$

A study of reaction (4a) on the basis of the $p\pi^+$ mass distribution alone cannot take into account the influence of $p\pi^+\pi^-$ resonances. For kinematical reasons, resonances at low $p\pi^+\pi^-$ masses give rise to enhancements at low $p\pi^+$ masses. Also, if a higher isobar in $p\pi^+\pi^-$ decays via $\Delta^{++}\pi^-$,

$$p\bar{p} \rightarrow N^*p \rightarrow (\Delta^{++}\pi^-)p \rightarrow (p\pi^+\pi^-)p, \quad (4b)$$

then this reaction cannot be separated from reaction (4a) by considering only the $p\pi^+$ distribution.

In order to relate the $p\pi^+$ analysis to the $p\pi^+\pi^-$ mass distribution, the latter distribution was divided into 24 mass intervals, each 100 MeV wide. A maximum-likelihood program MITOSIS analyzed the events of each of these intervals [see Fig. 8(a)] and determined the number of events whose $p\pi^+$ masses are distributed according to a Breit-Wigner³¹ distribution ($M_0=1236$ MeV, $\Gamma=120$ MeV) by considering the three-dimensional probability distribution

$$P(M(p\pi^+\pi^-), M(p\pi^+), M(p\pi^-)) \\ = \frac{M(p\pi^+)M(p\pi^-)}{M(p\pi^+\pi^-)} Q(p\pi^+\pi^-) \\ \times \left(N_{PS} \frac{1}{V_{PS}} + N_{\Delta^{++}} \frac{B(M(p\pi^+))}{V_{\Delta^{++}}} + N_{\Delta^0} \frac{B(M(p\pi^-))}{V_{\Delta^0}} \right).$$

Here Q is the c.m. momentum of the $p\pi^+\pi^-$ combination considered, $B(M)$ is the Breit-Wigner distribution, and the V 's are normalization constants. The N_{PS} , $N_{\Delta^{++}}$, and N_{Δ^0} are the number of events in a given interval that are distributed according to phase space, Δ^{++} and Δ^0 , respectively. Summing over intervals, this method yields a total cross section for Δ^{++} production of $\sigma(\Delta^{++}) = 1.31 \pm 0.14$ mb (all processes). For the Δ^0 production, which is obviously weaker [Figs. 7 and 11(a)], the MITOSIS analysis yielded no significant results in the individual mass intervals. These fits were repeated with additional factors included in the probability density to remove the discrepancy between the assumed $M(p\pi^+\pi^-)$ dependence of the three processes and the actual dependence observed in preliminary fits. The results of these modified fits were consistent with the preliminary fits for each $M(p\pi\pi)$ interval to well within the statistical error. The χ^2 value for the resulting $p\pi^+$ distribu-

tion (dashed curve of Fig. 7) is 106 for 85 histogram intervals. By means of this method the influence of the structure of the $p\pi^+\pi^-$ mass distribution on the $p\pi^+$

distribution is taken into account. Furthermore, one gets information on the distribution of Δ^{++} events within the $p\pi^+\pi^-$ mass distribution: The points in Fig.

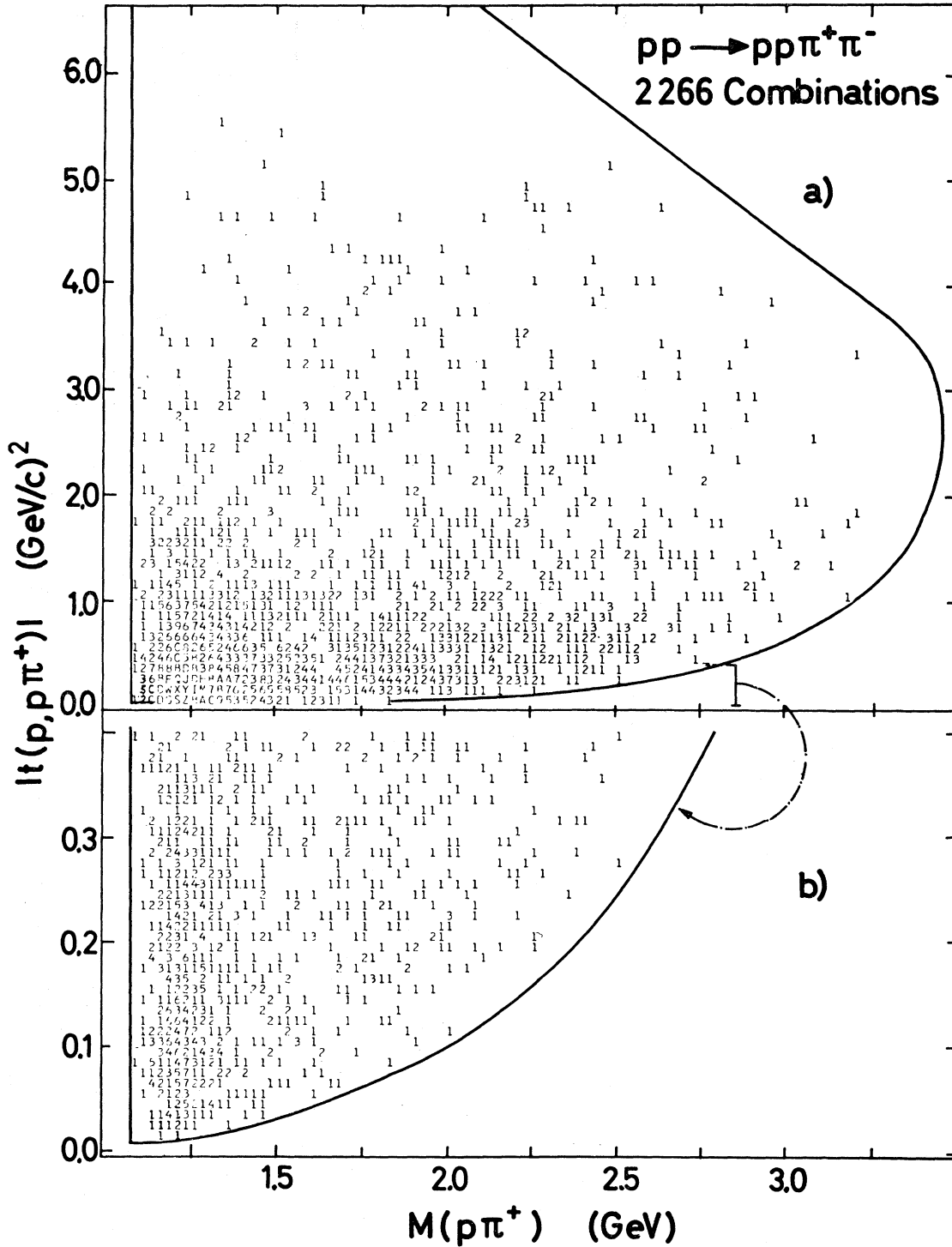


FIG. 7. Plots for the reaction $pp \rightarrow pp\pi^+\pi^-$. (a) Momentum transfer t to $p\pi^+$ versus $M(p\pi^+)$. The symbols A, B, C, ... mean 10, 11, 12, ... (b) Same as (a) with t scale expanded. (c) $M(p\pi^+)$ distribution; (d) Momentum transfer to $p\pi^+$ or $p\pi^-$. The full curve in (c) is calculated according to the OPFM and normalized to the number of events. The dashed curve is from the fit described in Sec. 7 A.

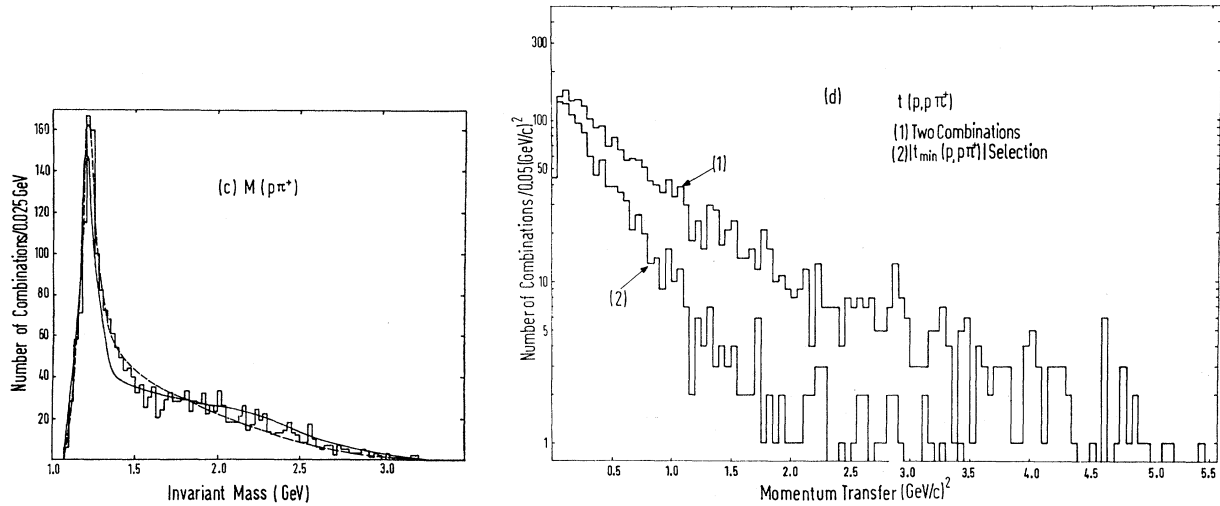


FIG. 7. (Continued)

8(a) show the value of $N_{\Delta^{++}}$ for each of the chosen $p\pi^+\pi^-$ mass intervals, and together they represent the $\Delta^{++}\pi^-$ mass distribution. They can be used for a comparison with the OPEM prediction for the shape of the $\Delta^{++}\pi^-$ distribution (Appendix B) for reaction (4a), shown by the lower curve in Fig. 8(a). The comparison shows that the $\Delta^{++}\pi^-$ mass distribution is well described by the OPEM over the whole mass region, except for the interval $1.65 \leq M(p\pi^+\pi^-) \leq 1.75$ GeV. Assuming the OPEM curve to be a valid background for reaction (4b), the deviation of 32 ± 18 events in that interval gives an estimate of the number of Δ^{++} due to reaction (4b). Subtracting these events from the total number of Δ^{++}

analyzed, we obtain a best estimate of $\sigma = 1.25 \pm 0.14$ mb for reaction (4a).

Conventional least-squares analysis of the $p\pi^+$ distribution alone, using Lorentz-invariant phase space and a Breit-Wigner resonance multiplied by Lorentz-invariant phase space, yielded a considerably larger (2.2–2.4 mb) cross section for Δ^{++} production. However, this method did not inspire confidence, because good fits (defined as having $\chi^2 < 115$, corresponding to a 1% confidence level) could be found only when we used a phase-space curve *not* modified to account for the observed t dependence of Δ^{++} production and allowed the fitted Δ^{++} mass to be in the region 1212–1214 MeV.

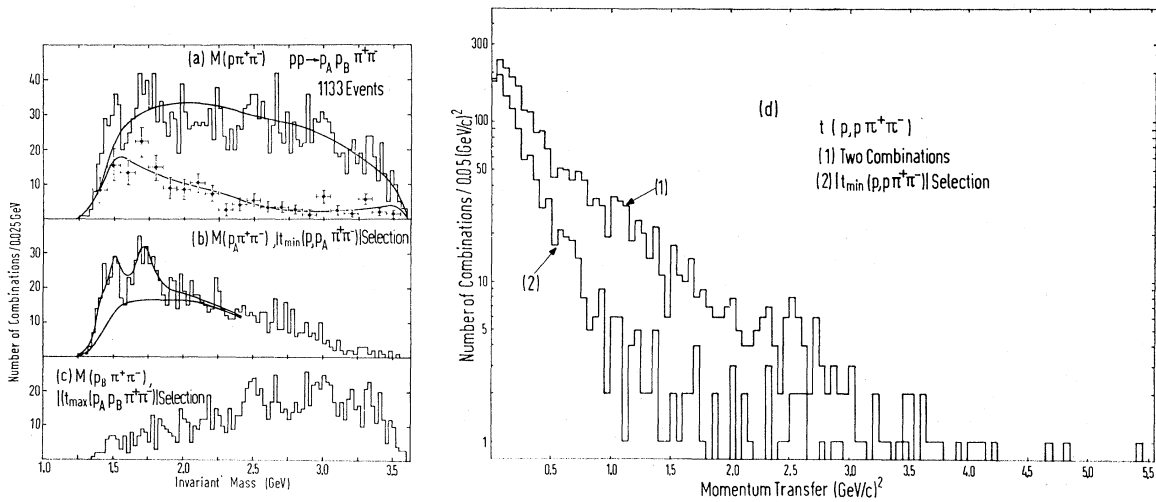


FIG. 8. Plots for the $p\pi^+\pi^-$ system. (a) Distribution of $M(p\pi^+\pi^-)$ (histogram) and of $M(\Delta^{++}\pi^-)$ (points) as determined in Sec. 7 A. The upper curve is calculated according to the OPEM and normalized to the number of events. The lower curve shows the prediction of the double-isobar diagram for $M(\Delta^{++}\pi^-)$. (b) Distribution of $M(p_A\pi^+\pi^-)$ (t_{\min} selection). The curve is from the fit described in Sec. 7 B. (c) Distribution of $M(p_B\pi^+\pi^-)$ (t_{\max} selection). (d) Distribution of four-momentum transfer to the $p\pi^+\pi^-$ system. The upper histogram contains both $p\pi^+\pi^-$ combinations, while the lower histogram contains only the t_{\min} -selected combination.

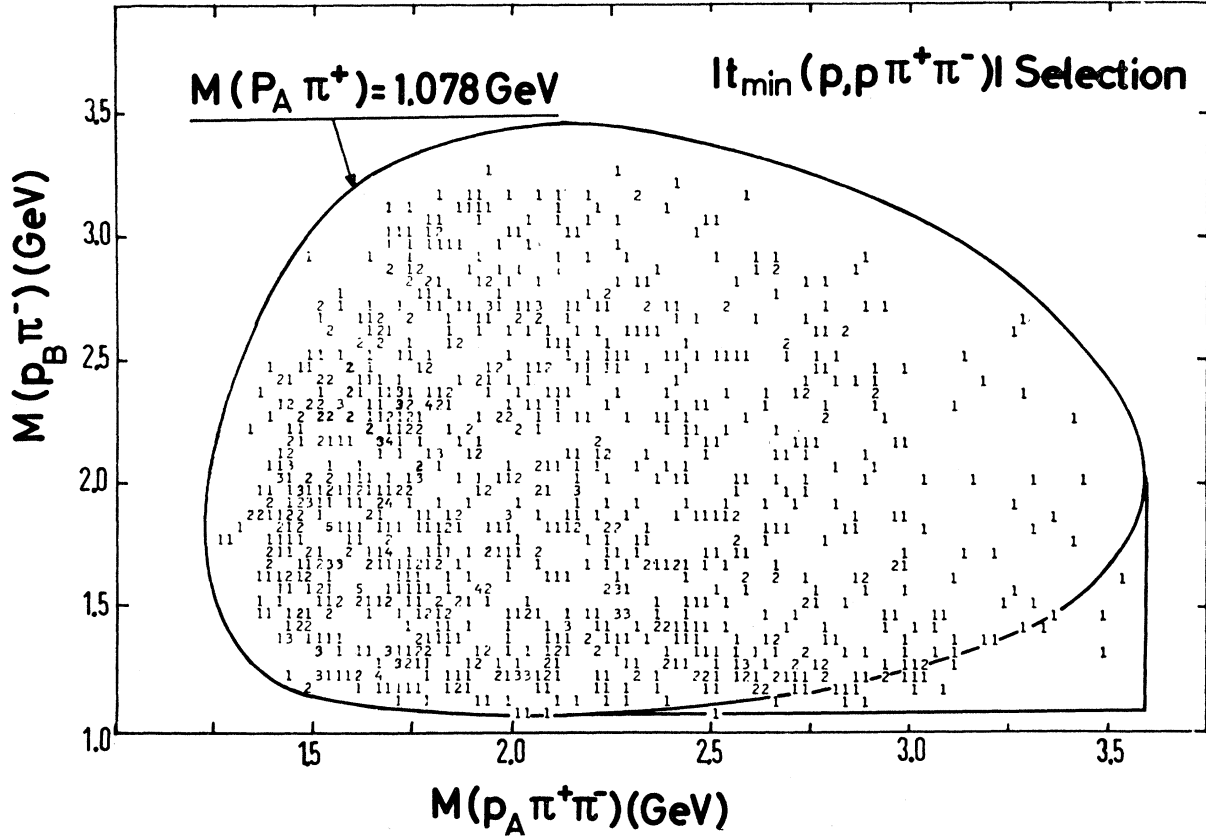


FIG. 9. Invariant masses $M(p_B\pi^-)$ versus $M(p_A\pi^+\pi^-)$ from the reaction $p\bar{p} \rightarrow p_B p_A \pi^+\pi^-$, where $p_A\pi^+\pi^-$ is the t_{\min} combination defined in the text, and curves for the kinematical boundaries.

B. Reaction $p\bar{p} \rightarrow pN^{*+} \rightarrow p(p\pi^+\pi^-)$

1. Selection of the Resonant Combinations

In reaction (4) there are two final-state $p\pi^+\pi^-$ combinations per event. Figure 8(a) shows the mass distribution for both combinations. If there is resonance production according to the reaction

$$p\bar{p} \rightarrow p_1 N^*, \quad N^* \rightarrow p_2 \pi^+\pi^-, \quad (4b)$$

then deviations of data from the OPEM curve in Fig. 8(a) arise from (a) the $N^*(p_2\pi^+\pi^-)$ resonances and (b) the "wrong" combinations $p_1\pi^+\pi^-$ of the same events. Selecting from each event that combination which is produced with the smallest momentum transfer (called the t_{\min} combination or $p_A\pi^+\pi^-$), we get the distribution shown in Fig. 8(b). The distribution of the other combination (called the t_{\max} combination or $p_B\pi^+\pi^-$) is shown in Fig. 8(c). The peaks at 1.5 and 1.7 GeV appear in the distribution of the t_{\min} combination only. Obviously this sample contains practically all of the resonant combinations. Because only one combination per event is plotted, Fig. 8(b) contains nearly no "wrong" combinations, which are then contained in the t_{\max} sample [Fig. 8(c)]. For the analysis of reaction (4b) only the combinations $p_A\pi^+\pi^-$ are therefore used.

2. Analysis of $p\pi^+\pi^-$ Resonances

An important question regarding reaction (4) is, to what extent the peaking at about 1.5 GeV in $p_A\pi^+\pi^-$ (Fig. 8) is caused by the Deck effect, that is, a kinematical enhancement arising from Δ^{++} production in reaction (4a) coupled with diffractive π^-p_B scattering. This point may be examined qualitatively by means of Fig. 9, which shows $M(p_A\pi^+\pi^-)$ plotted versus $M(p_B\pi^-)$. There is no indication that the events contributing to the 1.5-GeV peak are concentrated at high $p_B\pi^-$ masses, where diffractive π^-p scattering should be dominant. A more detailed discussion of this question¹¹ showed that the structure at 1.5 GeV cannot be explained completely by a model containing $\Delta^{++}(1236)$ production in the framework of the OPEM with form factors.³⁴ The use of this model for describing the Deck effect is supported by the general qualitative agreement between the OPEM curves and all mass distributions, and in particular by the results of Sec. 7 A which show the reliability of the OPEM calculation for reaction (4a).

³⁴ A reduction of this disagreement could be achieved in the above-mentioned experiment (Ref. 30) by using the Reggeized OPEM for $p\bar{p} \rightarrow \Delta^{++}p\pi^-$ by E. L. Berger, E. Gellert, G. A. Smith, E. Colton, and P. E. Schlein, Phys. Rev. Letters **20**, 964 (1968).

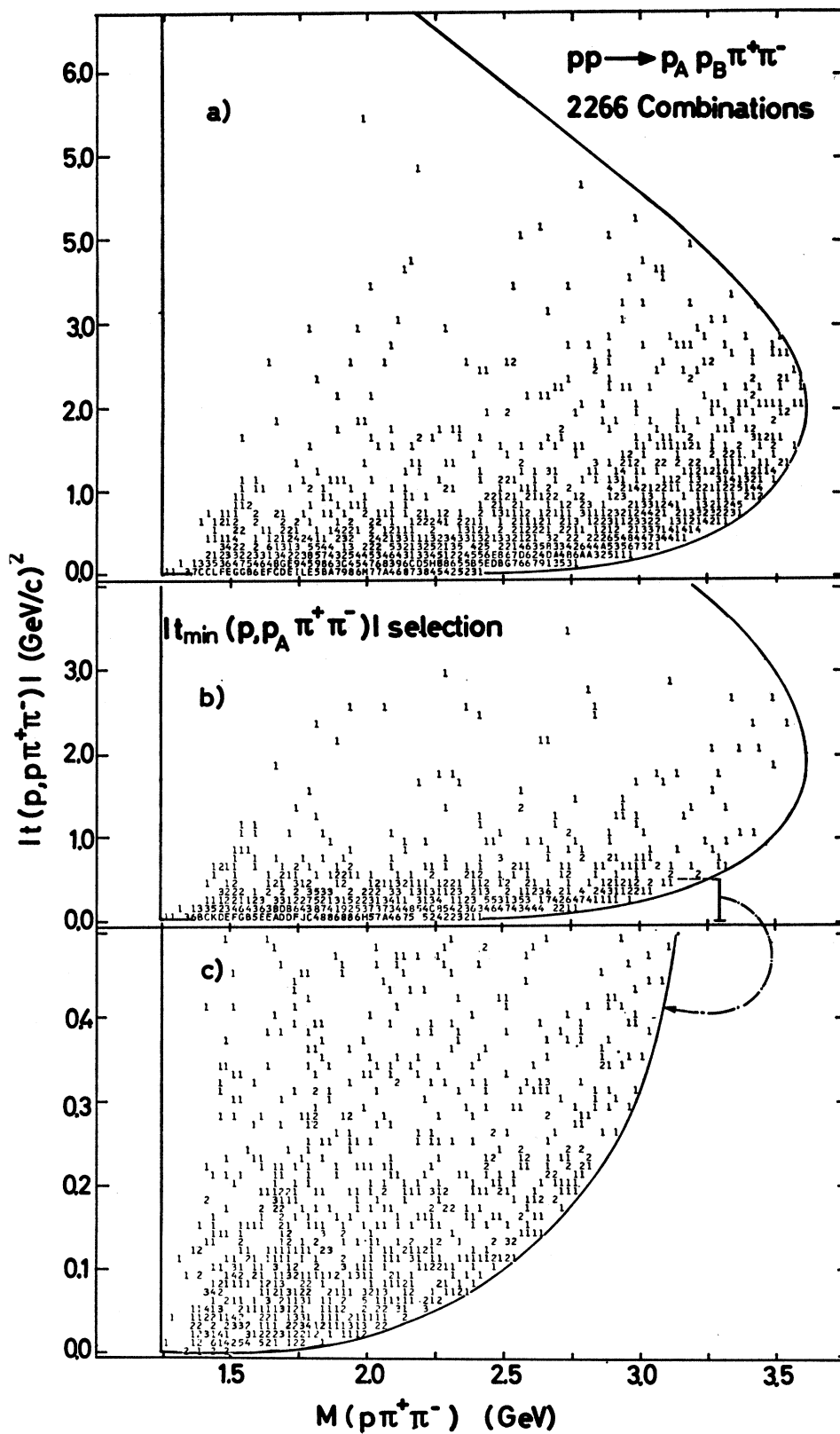


FIG. 10. Plots for the reaction $p\bar{p} \rightarrow p_A p_B \pi^+ \pi^-$.
 (a) Momentum transfer t to $p\pi^+\pi^-$ versus $M(p\pi^+\pi^-)$. The symbols A, B, C, ... mean 10, 11, 12, ...; (b) same as (a) but for the t_{\min} combination $p_A \pi^+ \pi^-$ only; (c) same as (b) with t scale expanded.

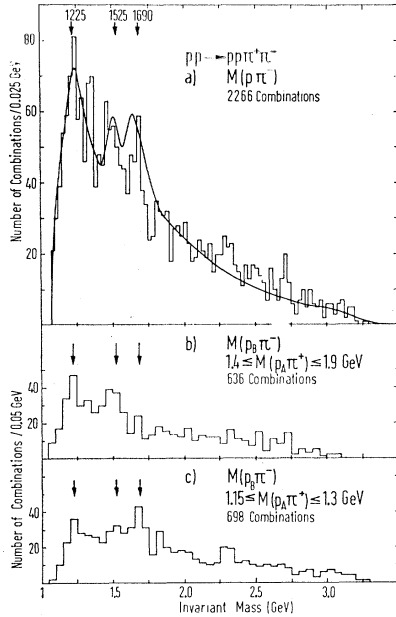


FIG. 11. Plots for the reaction $pp \rightarrow pp\pi^+\pi^-$. (a) Invariant mass for $p\pi^-$, all combinations; (b) $p_B\pi^-$ if $1.40 \leq M(p_A\pi^+) \leq 1.90$ GeV; (c) $p_B\pi^-$ if $1.15 \leq M(p_A\pi^+) \leq 1.30$ GeV.

Therefore, the OPEM prediction may be taken as a description of the nonresonant background for $p_A\pi^+\pi^-$, which fully takes into account the reflections from reaction (4a). However, the peak at 1.5 GeV cannot be explained simply in terms of OPEM background and the $N^*(1525)$ isobar: The Chew-Low plot in Fig. 10 shows that the t dependence of the $p_A\pi^+\pi^-$ distribution for events with a mass lower than 1.5 GeV is stronger than for events with higher masses. As shown in Ref. 11, a selection on momentum transfer split the 1.5-GeV peak into two peaks: one near 1.45 GeV for $|t| < 0.35$ (GeV/c)² and the other near 1.52 GeV, mainly in the remaining sample. This behavior is consistent with observations made in missing-mass experiments at a variety of incoming proton momenta (Refs. 6–9). Indeed, if we picture the final state of reaction (4) as a $p\pi^+\pi^-$ combination with mass $M(p\pi^+\pi^-)$ and momentum transfer t recoiling against a proton, our analysis of reaction (4) is directly comparable with missing-mass experiments. A rough estimate of the cross section for the peaks found in this experiment shows that they are consistent with those found in the missing-mass experiments. These experiments show that the differential production cross sections for these peaks, which are interpreted as $N^*(1400)$, $N^*(1520)$, and $N^*(1690)$ isobars in Refs. 6–8, are well described by

$$d\sigma/d|t| = A \exp(-b|t|),$$

with $b = 20, 4,$ and 5 (GeV/c)⁻², respectively. It is therefore possible to resolve the peak at 1.5 GeV by taking advantage of the very different t dependences of the resonances $N^*(1400)$ and $N^*(1520)$.

A maximum-likelihood program EMTE was used that analyzes the two-dimensional distribution $M(p_A\pi^+\pi^-)$ versus $t_{\min}(p, p_A\pi^+\pi^-)$ [Fig. 10(b)], in terms of distribution functions $F_i(M, t)$ for the three resonances ($i = 1, 2, 3$) and for two for the background ($i = 4, 5$). For the resonances, we use the relativistic Breit-Wigner formula

$$F_i(M) = \frac{M}{q} \frac{\Gamma(M)}{(M^2 - M_0^2)^2 + (\Gamma M_0)^2}$$

suggested by Jackson,³¹ generalized to include a t dependence: $F_i(M, t) = F_i(M) \exp(-b|t|)$. The widths of the resonances occurring in $F_i(M)$ were taken to be $\Gamma(M) = \Gamma_0 R_3(M) / R_3(M_{\text{Res}})$, where $R_3(M)$ is the volume of three-particle phase space with total energy M , and M_{Res} is the resonance mass.

The distribution functions for the background were constructed according to the OPEM for the two contributing diagrams (see Appendix B) separately. In the region $M(p_A\pi^+\pi^-) \simeq 1.5$ GeV the contribution $F_5(M, t)$ of the Drell diagram (Fig. 22, diagram 4) is about 10% of the contribution F_4 of the double-isobar diagram (Fig. 22, diagram 3). The t dependence of the latter is roughly $\exp(-10|t|)$ (in GeV) in this mass region. The t dependence of $F_4(M, t)$ was analyzed in a preliminary fit to the data. The result was in good agreement with the distribution predicted by the OPEM calculation. The total distribution function is

$$F(M, t) = \sum_{i=1}^5 N_i F_i(M, t),$$

where N_i corresponds to the number of events for distribution i . The results of the fit are given in Table V.

3. Decay of $N^*(p\pi^+\pi^-)$ Resonances

From the distribution of the $\Delta^{++}\pi^-$ over the $p\pi^+\pi^-$ mass spectrum [Fig. 8(a)] one can obtain some information on the decay of the $p\pi^+\pi^-$ resonances through $\Delta^{++}\pi^-$. The visible decay via $\Delta^0\pi^+$ for resonances with $T = \frac{1}{2}$ is $\frac{1}{3}$ of the decay $\Delta^{++}\pi^-$ and is therefore not considered. Attributing the excess of the $\Delta^{++}\pi^-$ points [Fig. 8(a)] over the OPEM curve in the regions of the $N^*(p\pi^+\pi^-)$ to these resonances, and assuming the OPEM curve to be an exact representation of the back-

TABLE V. Results of fit to the $p\pi^+\pi^-$ mass and momentum-transfer distribution.

| Resonance | Mass (MeV) | Width (MeV) | b (GeV/c) ⁻² | Cross section (mb) |
|-----------------|-------------------|------------------|--------------------------------------|--------------------|
| (1) $N^*(1450)$ | 1450 ± 17 | 210 ^a | 20.8 ± 4.5 | 0.18 ± 0.04 |
| (2) $N^*(1525)$ | 1525 ^b | 105 ^b | 4 ^c | 0.15 ± 0.04 |
| (3) $N^*(1700)$ | 1734 ± 21 | 140 ± 57 | 5 ^c | 0.22 ± 0.07 |

^a Estimates of the width found in the literature [Refs. 32(b), 36, and 37] range between 180 and 260 MeV. The errors quoted for the fitted quantities in Table V take into account this uncertainty, as well as the usual statistical errors.

^b Values from Ref. 38.

^c Values from Ref. 6.

TABLE VI. Partial cross sections in mb for reaction $p p \rightarrow p p \pi^+ \pi^-$.

| Reaction | Cross section ^a |
|--|----------------------------|
| $p p \rightarrow \Delta^{++} p \pi^-$ | 1.25 ± 0.14 |
| $p p \rightarrow p \pi^+ \Delta^0$ | 0.29^b |
| $p p \rightarrow p \pi^+ N^{*0}(1525)$ | 0.15^b |
| $p p \rightarrow p \pi^+ N^{*0}(1690)$ | $0.16^{b,c}$ |
| $p p \rightarrow N^{*+}(1450) p$ | 0.18 ± 0.04 |
| $p p \rightarrow N^{*+}(1525) p$ | 0.15 ± 0.04 |
| $p p \rightarrow N^{*+}(1700) p$ | 0.22 ± 0.07 |
| $p p \rightarrow p p f^0$ | 0.064 ± 0.027 |

^a Cross sections given in this table refer only to those decays of the resonances involved, which lead to the final state $p p \pi^+ \pi^-$.

^b Errors are estimated to be about 40%.

^c Strongly correlated with Δ^{++} production.

ground, the following estimates of the branching ratio R are obtained:

$$R = \frac{N^{*+} \rightarrow \Delta^{++} \pi^-}{N^{*+} \rightarrow p \pi^+ \pi^- (\text{all modes})},$$

$$N^*(1450), \quad R = 0.0_{-0.0}^{+0.3},$$

$$N^*(1525), \quad R = 0.0_{-0.0}^{+0.3},$$

$$N^*(1700), \quad R = 0.31 \pm 0.17.$$

Possible systematic errors due to the assumptions made in the OPEM calculations and in the MITOSIS analysis are difficult to determine and have not been included in these errors. Investigations of the decay of higher isobars have also been carried out by the other authors.³⁵

C. Resonances in $p \pi^-$

In the $p \pi^-$ mass distribution (Fig. 11) peaks are to be seen at about 1.22, 1.49, and 1.69 GeV. The peaks are not significant enough for an analysis similar to that applied to the reaction $p p \rightarrow p \Delta^{++} \pi^-$ (Sec. 7 A), and because of the lack of a reliable description of the non-resonant background, fits to the $p \pi^-$ distribution alone are not feasible. Therefore only visual estimates are given in Table VI.

From the data it is not clear whether the peak at 1.49 GeV may be exclusively $N^*(1525)$ production, or if other effects contribute to it. In other experiments^{3,4(a)} the corresponding peak appears centered at a mass near 1.48–1.50 GeV.

Inspection of the triangle plot $M(p_A \pi^+)$ versus $M(p_B \pi^-)$ (Fig. 12) shows no correlation between $\Delta^{++}(1236)$ production and the resonances at 1.22 and 1.49 GeV. However, the events giving rise to the peak

³⁵ G. Alexander, O. Benary, B. Haber, N. Kidron, A. Shapira, G. Yekutieli, and E. Gotsman, *Nuovo Cimento* **40**, 839 (1965); Ref. 1; V. Alles-Borelli, B. French, A. Frisk, and L. Michejda, *Nuovo Cimento* **47A**, 232 (1967); O. Czyzewski, B. Escoubès, Y. Goldschmidt-Clermont, M. Guinea-Moorhead, D. R. O. Morrison, and S. de Unamuno-Escoubès, *Phys. Letters* **20**, 554 (1966); H. L. Kraybill, D. L. Stonehill, B. Deler, W. Laskar, J. P. Merlo, G. Valladas, and G. W. Tautfest, *Phys. Rev. Letters* **16**, 863 (1966); Y. Y. Lee, W. D. C. Moebis, B. P. Roe, D. Sinclair, and J. C. Vander Velde, *Phys. Rev.* **159**, 1156 (1967).

at 1.69 GeV appear to be strongly correlated with the Δ^{++} peak, indicating the presence of one or more reactions of the type $p p \rightarrow \Delta^{++}(1236) N^*(1690)$. We may exclude the possibility of the reaction $p p \rightarrow \Delta^{++}(1236) \Delta^0(1670)$, because we see no evidence for the charge-symmetric final state $\Delta^0(1236) \Delta^{++}(1670)$, which would be present in equal strength. The $N^*(1690)$ must therefore be one or more of the $T = \frac{1}{2}$ states.^{32(b),36–38}

D. Resonances in $\pi^+ \pi^-$

In the $\pi^+ \pi^-$ mass distribution [Fig. 6(b)] an indication of possible f^0 production is seen. An estimate of the cross section for possible f^0 production by means of a fit to a superposition of background curve (shape according to the OPEM prediction) and a Breit-Wigner resonance with fixed mass and width ($M = 1254$ MeV, $\Gamma = 117$ MeV³⁸) in the mass region $1.0 \leq M(\pi^+ \pi^-) \leq 1.7$ GeV yielded

$$\sigma(p p \rightarrow p p f^0 \rightarrow \pi^+ \pi^-) = 64 \pm 27 \mu\text{b}.$$

This amounts to a 2.4-standard-deviation signal. Hence production of f^0 is not established in this experiment and the above cross section is to be taken as an upper limit. Because the $\pi^+ \pi^-$ mass distribution varies strongly in the ρ region, it is not possible to give reasonable upper or lower limits for ρ production.

E. Comparison with the OPEM

Because the use of the OPEM is essential in some of the previous fits, we discuss here the reliability of this model.

1. Qualitative Evidence for OPEM

The OPEM for reaction (4) considers the diagrams 3 and 4 (Fig. 22) of Appendix B. The qualitative evidence that these diagrams are playing a role is as follows:

(a) Apart from important deviations in the $p \pi^+ \pi^-$ mass distribution, the OPEM calculations for all mass distributions are qualitatively in agreement with experiment. Ordinary Lorentz-invariant phase space or phase space modified by peripheral effects disagree with the experimental distributions.

(b) The shape parameters A_1/A_0 , defined by Gellert *et al.*³⁰ [also discussed in Sec. 6, in connection with reaction (3)], have been calculated as a function of $M(p \pi^+)$ for events with $p \pi^+$ produced at small angles: $\cos \theta(p_{\text{in}}, p \pi^+) \geq 0.965$ [Fig. 13(a)]. For $p_B \pi^-$ the A_1/A_0 have been calculated with the additional restriction that

³⁶ L. D. Roper, *Phys. Rev. Letters* **12**, 340 (1964).

³⁷ C. Lovelace [CERN Report No. TH 705, 1966 (unpublished)] gives a complete list of references with critical remarks. For subsequent work, see Ref. 32b; C. Lovelace, in *Proceedings of the Heidelberg International Conference on Elementary Particles*, edited by H. Filthuth (Interscience Publishers, Inc., New York, 1968), p. 79.

³⁸ A. H. Rosenfeld, N. Barash-Schmidt, A. Barbaro-Galtieri, W. J. Podolsky, L. R. Price, P. Söding, Ch. G. Wohl, M. Roos, and W. J. Willis, *Rev. Mod. Phys.* **40**, 77 (1968).

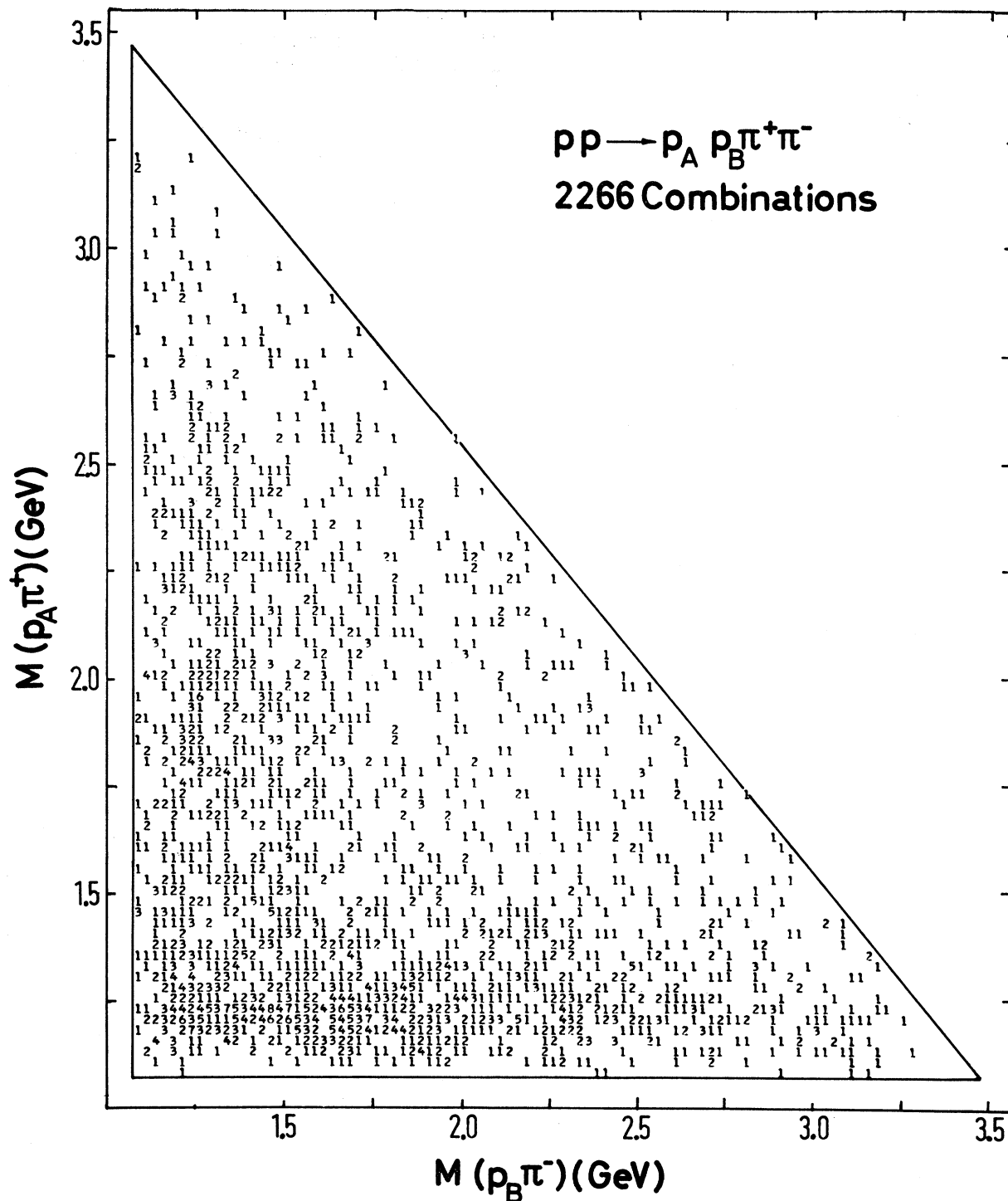


FIG. 12. Invariant masses $M(p_A\pi^+)$ versus $M(p_B\pi^-)$, two combinations per event.

$M(p_A\pi^+)$ be in the Δ^{++} region $1.125 \leq M(p_A\pi^+) \leq 1.325$ [Fig. 13(b)]. The curves shown in Fig. 13 are calculated from experimental data on free $p\pi^\pm$ scattering.³² In the paper of Gellert *et al.*,³⁰ qualitative agreement between the curves and experimental points was interpreted as

evidence that the OPEM plays a major role in reaction (4) at 6.6 GeV/c. We find similar qualitative agreement. Since the curves are not corrected for off-shell effects or background events (see Sec. 7 A), complete agreement is not to be expected.

(c) The total cross section for the reaction, calculated from diagrams 3 and 4 (Appendix B, Fig. 22), can be brought into agreement with our experiment, using form factors consistent with those derived at other energies and from other reactions.^{39,40}

2. Check of the Double-Isobar Diagrams

The evaluation of the double-isobar diagram (diagram 3, Fig. 22, Appendix B) is carried out using well-established physical elastic cross sections, whereas the treatment of the Drell diagram (diagram 4) is to be considered as a rough approximation. Therefore a quantitative check of the OPEM is meaningful only for the double-isobar diagram and comparison with experiment must be confined to a kinematical region where the contribution from the double-isobar diagram is much larger than that from the Drell diagram.

Furthermore, the definite deviations from the OPEM predictions mentioned above (Sec. 7 B) indicate the presence of additional reactions. In our comparison with the double-isobar diagram the contributions of these other effects must be explicitly accounted for. These conditions are approximately fulfilled in the following two comparisons that we made after having chosen $\gamma = 30\mu^2$ to get agreement between theoretical and experimental cross sections for $p p \rightarrow p \pi^+ \Delta^{++}$:

(a) In Fig. 8(a), we compare the prediction of the OPEM with the experimental points for $d\sigma/dM(\Delta^{++}\pi^-)$. The agreement is good.

(b) In Sec. 7 B, the contribution of the double-isobar diagram is considered in the fit to the Chew-Low plot [Fig. 10(b)] and represented by the two-dimensional distribution $d^2\sigma/(dM dt) \sim F_4(M, t)$. For masses $M \leq 2.4$ GeV, the contribution of the double-isobar diagram is, on the average, three times larger than that of the Drell diagram. In that mass region a fit that considered all distributions simultaneously allowed the slope of the t dependence for $F_4(M, t)$ to be modified. Best agreement with the data was achieved with the unmodified t dependence of the double-isobar diagram.

Thus the use of the OPEM in the analysis of reaction (4) would seem justified.

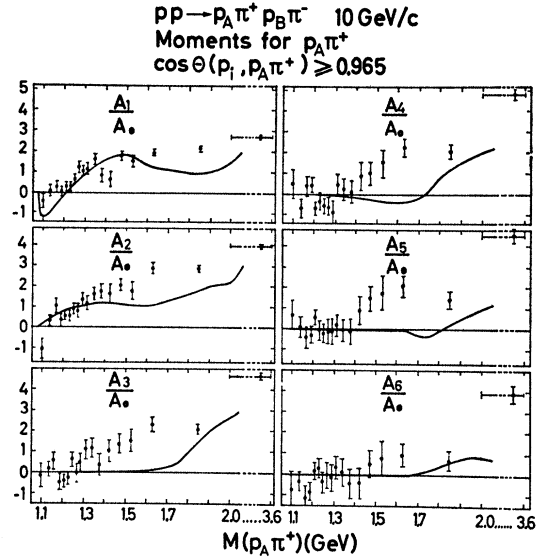
8. REACTION $p p \rightarrow p p \pi^+ \pi^- \pi^0$

The analysis of the one-C four-prong reaction channels is made difficult by large fractions of ambiguous hypotheses. The main contributions to the ambiguities and the methods used to get a clean sample of events are the following:

(a) About 4% of the events that gave a fit to the reaction $p p \rightarrow p p \pi^+ \pi^- \pi^0$ also gave a four-C fit to the re-

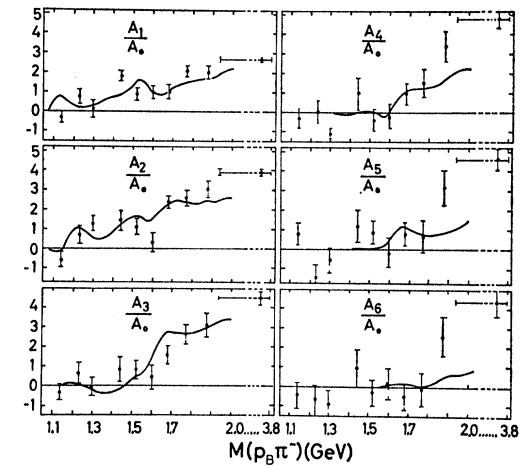
³⁹ E. Ferrari and F. Selleri, Nuovo Cimento **27**, 1450 (1963).

⁴⁰ O. Czyzewski, B. Escoubès, Y. Goldschmidt-Clermont, M. Guinea-Moorhead, T. Hofmökler, D. R. O. Morrison, and S. de Unamuno-Escoubès, in *Proceedings of the Twelfth International Conference on High-Energy Physics, Dubna, 1964*, (Atomizdat, Moscow, 1965), Vol. I, p. 148.



(a)

PP \rightarrow $p_A \pi^+ p_B \pi^-$ 10 GeV/c
Moments for $p_B \pi^-$
 $\cos \theta(p_i, p_B \pi^-) \geq 0.965$ $1.160 \leq M(p_A \pi^+) \leq 1.280$ GeV



(b)

FIG. 13. Shape parameters in the reaction $p p \rightarrow p p \pi^+ \pi^-$. (a) For the $p_A \pi^+$ vertex of events with $|\cos \theta(p_i, p_A \pi^+)| \geq 0.965$. (b) For the $p_B \pi^-$ vertex of events with $|\cos \theta(p_i, p_B \pi^-)| \geq 0.965$ and $1.16 \leq M(p_A \pi^+) \leq 1.28$ GeV. θ is the production angle of the $p \pi$ system. Smooth curves are the shape parameters derived from free πp elastic scattering.

action $p p \rightarrow p p \pi^+ \pi^-$. These events were rejected from the one-C sample and assigned to reaction (4) on the basis of the FAKE results.

(b) In about $\frac{1}{3}$ of the events more than one one-C hypothesis gave a fit. The inspection of the c.m. angular distribution of the nucleons in these events and in the events that gave a fit to only one hypothesis led to the following criterion: The hypothesis with the strongest forward-backward alignment of the nucleons was selected to be the true hypothesis; all others were re-

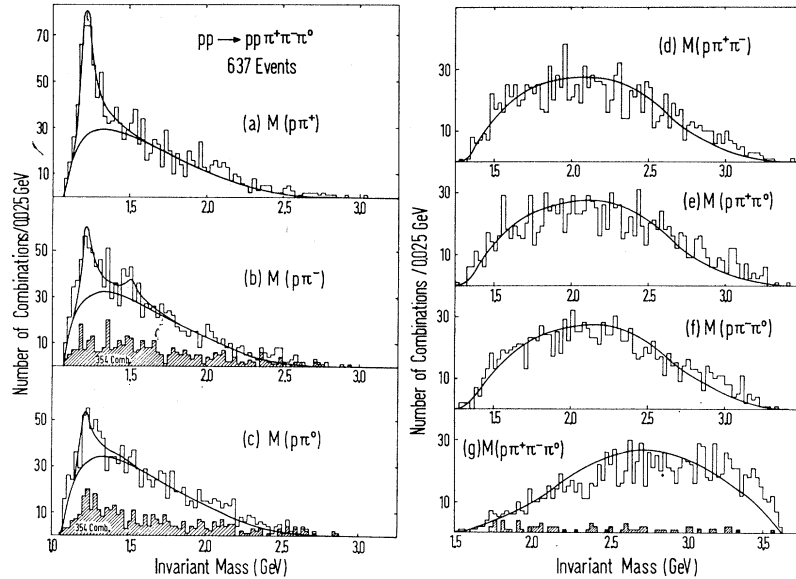


FIG. 14. Invariant-mass distributions for $pp \rightarrow pp\pi^+\pi^-\pi^0$. (a) $p\pi^+$; (b) $p\pi^-$; (c) $p\pi^0$; (d) $p\pi^+\pi^-$; (e) $p\pi^+\pi^0$; (f) $p\pi^-\pi^0$; (g) $p\pi^+\pi^-\pi^0$. The shaded histograms in (b) and (c) are $p_b\pi^-$ and $p_b\pi^0$ combinations for events with $p_a\pi^+$ in the Δ^{++} region (1.15–1.30 GeV). The shaded histogram in (g) is for events with $\pi^+\pi^-\pi^0$ in the ω region (0.76–0.80 GeV).

jected. In most cases the selected hypothesis was the one with the lowest χ^2 value.

(c) Another 12% of the events were deleted from the sample. These events, when fitted to the hypothesis $pp \rightarrow pp\pi^+\pi^-\pi^0$, had a π^0 going in the extreme forward direction with high momentum and probably came from a no-fit channel with a neutron going forward with high momentum.

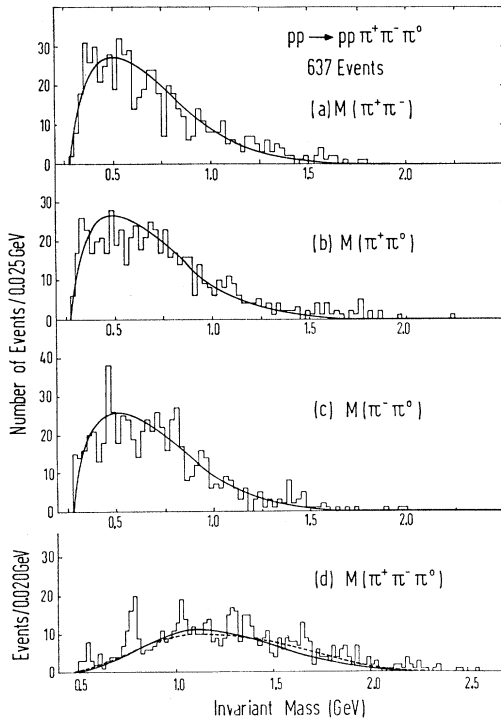


FIG. 15. Invariant-mass distributions for $pp \rightarrow pp\pi^+\pi^-\pi^0$. (a) $\pi^+\pi^-$; (b) $\pi^+\pi^0$; (c) $\pi^-\pi^0$; (d) $\pi^+\pi^-\pi^0$.

The remaining sample consists of 637 events. The contamination from other channels is estimated to be about 10%, and the fraction of true events rejected by the above procedure is somewhat less than 5%.

The invariant-mass distribution of the various particle combinations that contain one proton are given in Fig. 14. There is clear evidence for the production of the $\Delta(1236)$ and possible evidence for the production of the $N^*(1525)$.

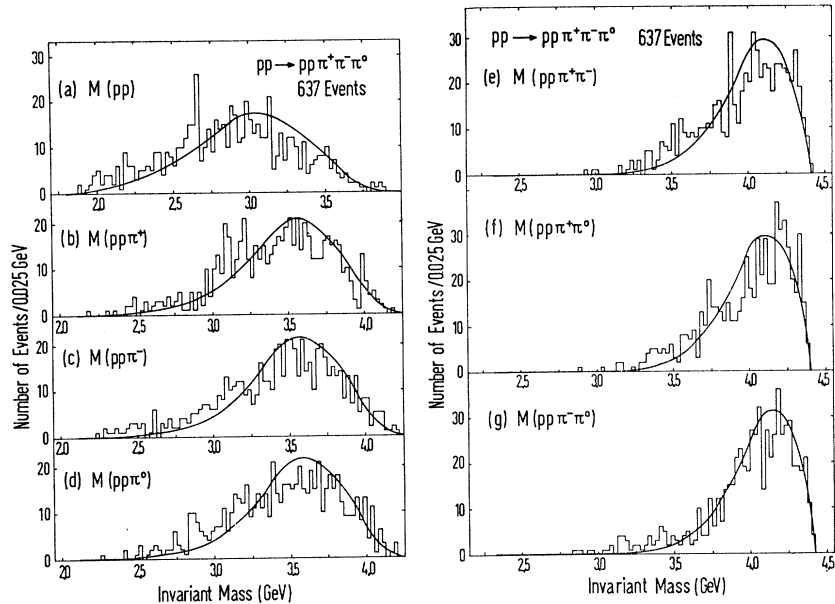
Since Lorentz-invariant phase space fails to give a reasonable description of the background, we used the method described in Sec. 4 to calculate background curves. These curves are in good agreement with the histograms for combinations without strong-resonance production, and are also in rough agreement with curves calculated for the same distributions with the OPEM with form factors using diagrams 5–7 given in Fig. 22. The kinematical reflections caused by resonance production are calculated with the model described in Sec. 4, except that the randomly generated events are given a weighting factor proportional to the Breit-Wigner curve for the resonant combination.

In order to determine the fractions of events in which the $\Delta(1236)$ and/or the $N^*(1525)$ is produced, the histogram of the invariant mass was fitted by a least-squares method to the equation

$$N(M)[f_{nr} + f_{\Delta}B_{\Delta}(M) + f_{N^*}B_{N^*}(M)]\theta(M),$$

where $N(M)$ is the number of events in the interval at mass M , $\theta(M)$ is the value of the background curve, and f_{nr} , f_{Δ} , and f_{N^*} are fractions of nonresonant and resonant terms in the distribution, assuming incoherent addition of resonant and nonresonant terms. $B_{\Delta}(M)$ and $B_{N^*}(M)$ are the (normalized) enhancement factors defined by Jackson.³¹

FIG. 16. Invariant-mass distributions for $pp \rightarrow pp\pi^+\pi^-\pi^0$. (a) pp ; (b) $pp\pi^+$; (c) $pp\pi^-$; (d) $pp\pi^0$; (e) $pp\pi^+\pi^-$; (f) $pp\pi^+\pi^0$; (g) $pp\pi^-\pi^0$.



The results of the fit to the histograms in the region $1.1 < M(p\pi) < 2.0$ GeV with resonance masses held fixed at the values of 1.236 and 1.525 GeV, respectively, and widths held fixed at the values of 0.120 and 0.105 GeV, respectively, are shown in Figs. 14(a)–14(c). The partial cross sections obtained by the fit are given in Table VII.

No appreciable double-isobar production is present in this reaction, as is seen from Figs. 14(b) and 14(c), where $p\pi^-$ and $p\pi^0$ mass combinations are plotted for events with $p\pi^+$ in the isobar region 1.15–1.30 GeV [shaded histogram in Figs. 14(b) and 14(c)].

The $p\pi\pi$ and $p\pi\pi\pi$ invariant-mass distributions [Figs. 14(d)–14(g)] are well described by the curves shown, which include reflections from $\Delta(1236)$ production according to the partial cross sections given in Table VII, and an appropriate fraction of background, and are normalized to the number of events in the histograms. The main influence of the reflection from $\Delta(1236)$ production is a broad enhancement in the $p\pi\pi$ mass distributions below 2.0 GeV, coming from $\Delta\pi$ combinations.

The two- and three-pion effective-mass distributions are given in Fig. 15. The curves are a superposition of background and reflections from $\Delta(1236)$ production. The two-pion effective-mass distributions do not show any indication for ρ or other resonance production. There is evidence for ω production and some η production in the $\pi^+\pi^-\pi^0$ mass distribution [Fig. 15(d)]. The full curve in this figure is calculated with the model described in Sec. 4. The dashed curve is calculated with the OPEM with form factors using diagrams 5–7 in Fig. 22; both curves are normalized to the number of nonresonant events with mass $M(\pi^+\pi^-\pi^0)$ below 1.0 GeV and fail to give a satisfactory description of the higher-mass region. We checked that the peak at 1030

MeV is not due to ϕ production by fitting all four-prong events to the reaction $pp \rightarrow ppK^+K^-$. No ϕ was seen in the resulting K^+K^- mass distribution, giving an upper limit of $12 \mu\text{b}$ for the reaction $pp \rightarrow pp\phi$. The observed width at half-maximum for the ω is 40 MeV, giving an estimate of the experimental resolution in this final state. Cross sections for ω and η production are given in Table VII. The $p\pi^+\pi^-\pi^0$ invariant-mass distribution for events with $\pi^+\pi^-\pi^0$ invariant mass in the ω region [shaded histogram in Fig. 14(g)] does not show any evidence for a $p\omega$ resonance.

The remaining invariant-mass distributions are shown in Fig. 16, together with curves that are a superposition of reflections from Δ production and of a background calculated as described in Sec. 4.

9. REACTION $pp \rightarrow pn\pi^+\pi^+\pi^-$

The ambiguities in this reaction are somewhat more frequent than in the other one-C-fit reaction $pp \rightarrow pp\pi^+\pi^-\pi^0$. Nearly one-half of the events that gave a fit to a hypothesis $pp \rightarrow pn\pi^+\pi^+\pi^-$ also gave a fit to another one-C hypothesis, most frequent of the same

TABLE VII. Partial cross sections in mb for reaction $pp \rightarrow pp\pi^+\pi^-\pi^0$.

| Reaction | Cross section ^a |
|---|----------------------------|
| $pp \rightarrow \Delta^{++}(1236)p\pi^-\pi^0$ | 1.02 ± 0.13 |
| $pp \rightarrow \Delta^+(1236)p\pi^+\pi^-$ | 0.42 ± 0.13 |
| $pp \rightarrow \Delta^0(1236)p\pi^+\pi^0$ | 0.58 ± 0.13 |
| $pp \rightarrow N^{*0}(1525)p\pi^+\pi^0$ | 0.14 ± 0.12 |
| $pp \rightarrow p\rho\omega^0$ | 0.145 ± 0.030 |
| $pp \rightarrow p\rho\eta^0$ | 0.036 ± 0.015 |

^a Cross sections given in this table refer only to those decays of the resonances involved, which lead to the final state $pp\pi^+\pi^-\pi^0$.

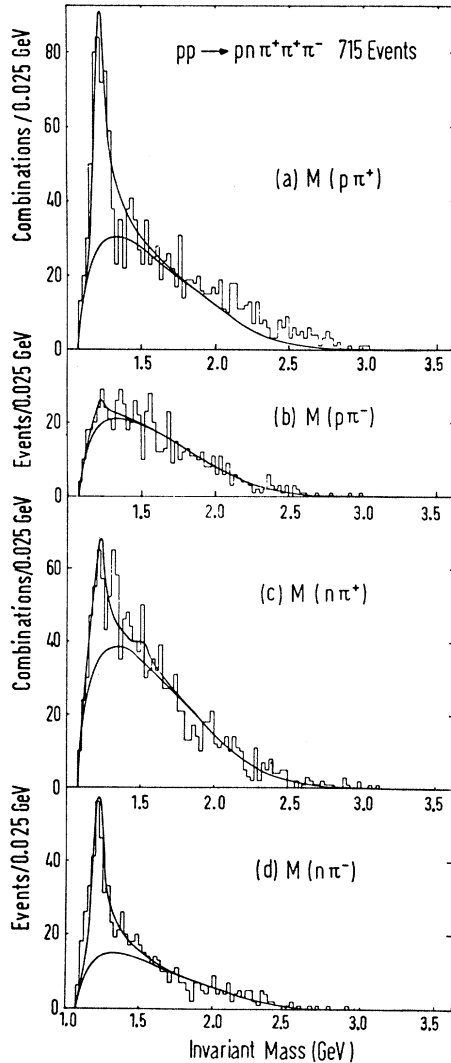


FIG. 17. Invariant-mass distributions for $pp \rightarrow pn\pi^+\pi^+\pi^-$. (a) $p\pi^+$ (two combinations per event); (b) $p\pi^-$; (c) $n\pi^+$ (two combinations per event); (d) $n\pi^-$.

reaction, i.e., with the outgoing proton and one π^+ interchanged. The same criteria as for the reaction $pp \rightarrow pp\pi^+\pi^-\pi^0$ (Sec. 8) were applied in these cases. In addition, criteria using the values of missing mass and χ^2

TABLE VIII. Partial cross sections in mb for reaction $pp \rightarrow pn\pi^+\pi^+\pi^-$.

| Reaction | Cross section ^a |
|---|----------------------------|
| $pp \rightarrow \Delta^{++}(1236)n\pi^+\pi^-$ | 1.11 ± 0.14^b |
| $pp \rightarrow \Delta^+(1236)p\pi^+\pi^-$ | 0.58 ± 0.14 |
| $pp \rightarrow \Delta^0(1236)n\pi^+\pi^+$ | 0.12 ± 0.07 |
| $pp \rightarrow \Delta^-(1236)p\pi^+\pi^+$ | 0.77 ± 0.10^b |
| $pp \rightarrow \Delta^{++}(1236)\Delta^-(1236)\pi^+$ | 0.57 ± 0.15 |
| $pp \rightarrow N^{*+}(1525)p\pi^+\pi^-$ | 0.07 ± 0.07 |
| $pp \rightarrow N^{*0}(1688)p\pi^+$ | 0.16 |

^a Cross sections given in the table refer only to those decays of the resonances involved, which lead to the final state $pn\pi^+\pi^+\pi^-$.

^b Including $\Delta^{++}\Delta^-$.

were applied to reduce the contamination coming from channels with more than one neutral particle in the final state. The contamination in the remaining sample, which consists of 715 events, is estimated to be about 15%, and about 10% of the true events are believed to be rejected by the criteria used.

The invariant-mass distributions of the various particle combinations that contain one nucleon are given in Figs. 17 and 18. The striking feature of the reaction is the production of the $\Delta(1236)$ in the isospin $|T_z| = \frac{3}{2}$ states [Figs. 17(a) and 17(d)], while production in the isospin state $|T_z| = \frac{1}{2}$ is smaller [Figs. 17(b) and 17(c)].

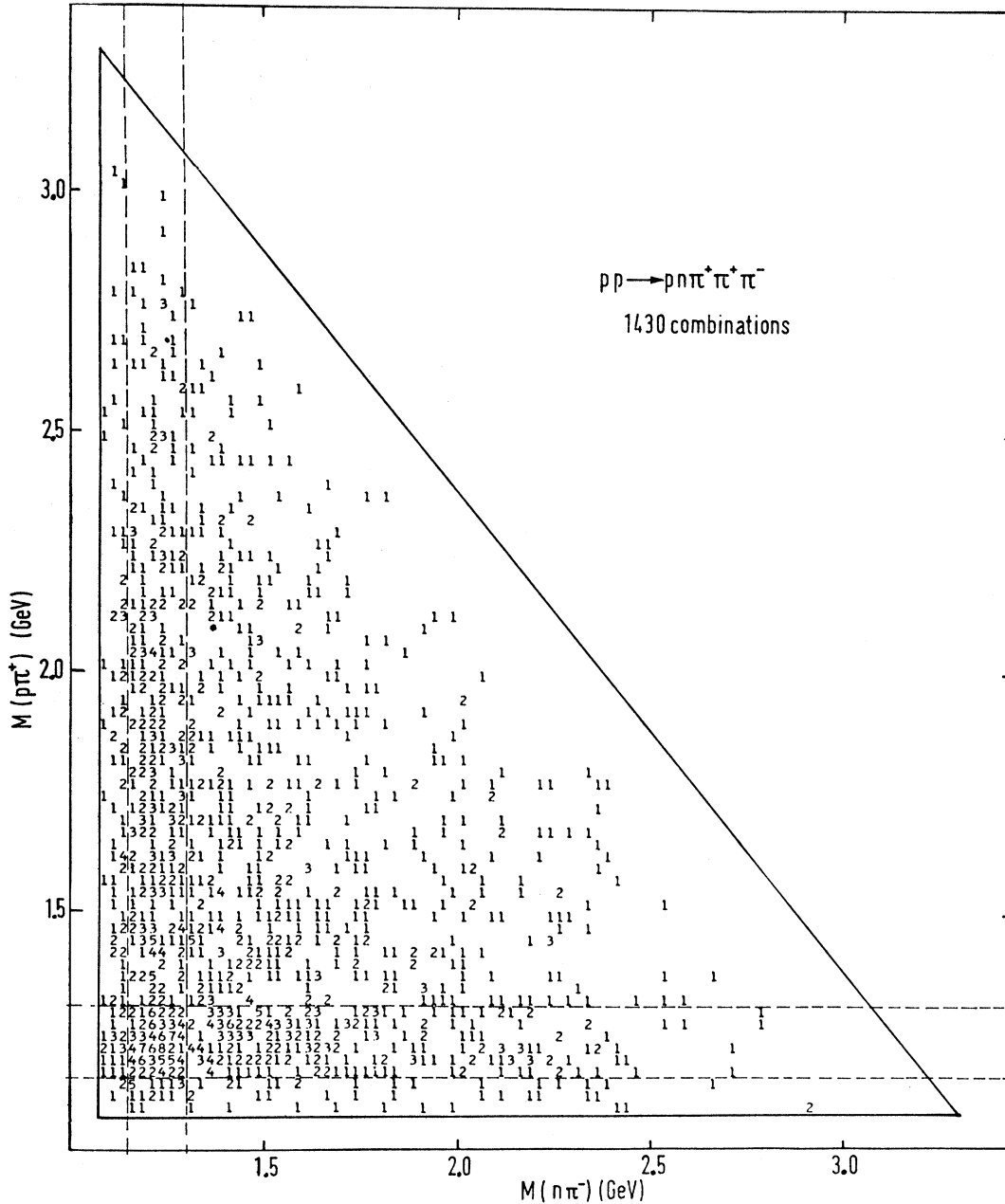
The method described in Sec. 8 was applied here in order to determine the fraction of events with $\Delta(1236)$ and $N^{*+}(1525)(n\pi^+)$. The results of the fits are shown in Figs. 17(a)–17(d).

Figure 18 shows the scatter plot $M(p\pi^+)$ versus $M(n\pi^-)$. We have estimated the amount of double-isobar production by examining the projections of the triangle plot. The $n\pi^-$ invariant-mass distribution was plotted for events having the $p\pi^+$ invariant mass in the isobar region (1.15–1.30 GeV) and in the adjacent region (1.3–1.5 GeV), respectively. The corresponding plots with the roles of $p\pi^+$ and $n\pi^-$ interchanged were also used. From these plots, double-isobar production is estimated to occur in 24% of the events. Cross sections for isobar production are presented in Table VIII.

The invariant-mass distributions for combinations with a nucleon and two pions are shown in Figs. 19(a)–19(d). The curves drawn in the figures include reflections from Δ production (only single-isobar production assumed) and an appropriate fraction of background, normalized to the total number of events.

A clear peak is seen in the $n\pi^+\pi^-$ mass combination at about 1.7 GeV, which is attributed to a three-body decay of one of the N^* resonances at this mass. The cross section for the reaction $pp \rightarrow p\pi^+N^*(1700)$ with subsequent N^* decay into $n\pi^+\pi^-$ is estimated to be 0.16 mb (by counting the number of events above the curve). This may be compared with the cross section of $\sigma = 0.16$ mb for the reaction $pp \rightarrow p\pi^+N^*(1700)$ with subsequent decay $N^* \rightarrow p\pi^-$ (Sec. 7). No evidence for an isospin $T = \frac{3}{2}$ isobar⁴¹ in the $p\pi^+\pi^+$ mass distribution is to be seen.

⁴¹ G. Goldhaber, S. Goldhaber, T. A. O'Halloran, and B. C. Shen, in *Proceedings of the Twelfth International Conference on High-Energy Physics, Dubna, 1964* (Atomizdat, Moscow, 1965); G. Alexander, O. Benary, B. Reuter, A. Shapira, E. Simonopoulou, and G. Yekutieli, *Phys. Rev. Letters* **15**, 207 (1965); Ref. 1. Recent evidence supporting the interpretation as a kinematic effect is given by G. Goldhaber, in *Proceedings of the Fourth Coral Gables Conference on Symmetry Principles at High Energy, 1967* (W. H. Freeman and Co., San Francisco, 1967); see also Ref. 14(a). No significant evidence has been found in Ref. 3. A $T = \frac{3}{2}$ isobar with a mass of 1650 MeV and a production cross section of $5 \mu\text{b}$ is claimed by M. Banner, M. L. Fayoux, J. L. Hamel, J. Cheze, J. Teiger, and J. Zsembery, in *Proceedings of the Heidelberg International Conference on Elementary Particles*, edited by H. Filthuth (Interscience Publishers, Inc., New York, 1968), p. 512; this agrees with the result of V. F. Vishnevskii, V. I. Moroz, A. V. Nikitin, and Yu. A. Trojan, Dubna Report No. P1. 3146, 1967 (unpublished).



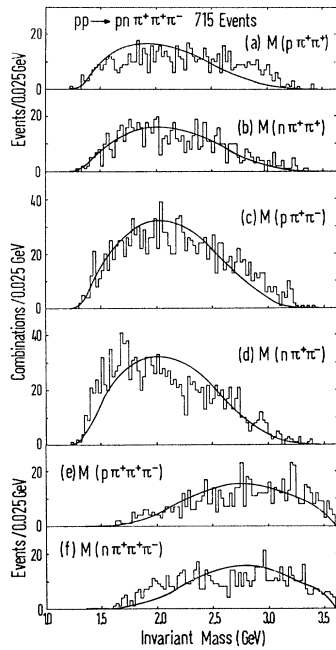


FIG. 19. Invariant-mass distributions for $pp \rightarrow pn\pi^+\pi^+\pi^-$. (a) $p\pi^+\pi^+$; (b) $n\pi^+\pi^+$; (c) $p\pi^+\pi^-$; (d) $n\pi^+\pi^-$; (e) $p\pi^+\pi^+\pi^-$; (f) $n\pi^+\pi^+\pi^-$.

value found for the total cross section $\sigma_{tot} = 41.1 \pm 1.7$ mb is in agreement with the values from counter experiments

The transverse momenta p_t of all particles in the reactions studied are rather small compared with the final-state nucleon longitudinal momenta that show forward-backward alignment along the incident-proton direction. Lorentz-invariant phase space, either unmodified or modified using the t dependence of some particle or combination of particles, gives poor agreement with our c.m.-momentum and invariant-mass distributions. A simple model in which the two components of transverse momentum of all particles and the longitudinal momenta of the pions are uncorrelated and normally distributed gives satisfactory agreement for channels with three pions in the final state. Therefore this model was used in the $pp\pi^+\pi^-\pi^0$ and $pn\pi^+\pi^+\pi^-$ channels as a background to investigate the production of meson and baryon resonances.

The elastic cross section is found to be 10.2 ± 0.9 mb.

In the discussion of the various channels it is shown that the gross features of the pion-production reactions studied can be explained by the OPEM with the form factors of Ferrari and Selleri.

A. $pp \rightarrow pn\pi^+$

Production of $\Delta^{++}(1236)$ accounts for about 30% of the reaction $pp \rightarrow pn\pi^+$. Small enhancements at 1480 MeV in $n\pi^+$ and 1900 MeV in $p\pi^+$ are also seen, which are tentatively interpreted as $N^*(1450)$ and $\Delta^{++}(1920)$. The cross sections are given in Table IV. The differ-

ential cross section $d\sigma/dt$ is in approximate agreement with OPEM calculations, using either the form-factor approach of Ferrari and Selleri or the absorption model with "extra" absorption. An analysis of the angular distribution of the outgoing p in the $p\pi^+$ c.m. system in terms of mean values of the spherical harmonics has also been made. There are statistically significant deviations from the values expected for the OPEM with form factors, suggesting that absorption and/or other meson exchanges are present.

B. $pp \rightarrow pp\pi^+\pi^-$

The characteristic features of the reaction $pp \rightarrow pp\pi^+\pi^-$ are its peripherality and the strong production of baryon resonances. There are two types of resonance-production channels: (a) $pp \rightarrow (p\pi^+)(p\pi^-)$ and (b) $pp \rightarrow p(p\pi^+\pi^-)$. Channel *a* with one or both indicated particle combinations in resonant states contributes 65% of the cross section for $pp \rightarrow pp\pi^+\pi^-$. This channel is dominated by the production of $\Delta^{++}(1236)$, which accounts for 50% of the cross section. The $\Delta^{++}(1236)$ production cross section is determined by an analysis of the three-dimensional distribution of $\{M(p\pi^+), M(p\pi^-), M(p\pi^+\pi^-)\}$. A determination from the $p\pi^+$ mass distribution alone led to inconsistent results. Resonance production according to channel *a* is described satisfactorily by the OPEM with form factors. Channel *b* contributes 23% of the cross section. $p\pi^+\pi^-$ resonances are found at 1.45, 1.52, and 1.73 GeV from an analysis of the Chew-Low plot. The 1.73-GeV $p\pi^+\pi^-$ resonance decays partly [(31±17)%] via $\Delta^{++}\pi^-$. The cross sections for these resonances and other fitted parameters

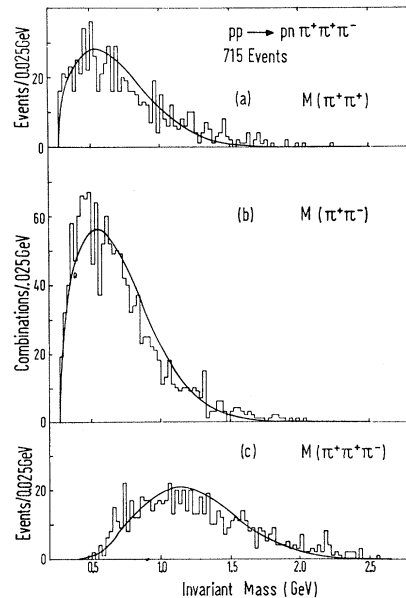


FIG. 20. Invariant-mass distributions for $pp \rightarrow pn\pi^+\pi^+\pi^-$. (a) $\pi^+\pi^+$; (b) $\pi^+\pi^-$; (c) $\pi^+\pi^+\pi^-$.

such as mass, width, and t dependence are given in Table V.

C. $p\bar{p} \rightarrow p\bar{p}\pi^+\pi^-\pi^0$ and $p\bar{p} \rightarrow pn\pi^+\pi^+\pi^-$

The reactions $p\bar{p} \rightarrow p\bar{p}\pi^+\pi^-\pi^0$ and $p\bar{p} \rightarrow pn\pi^+\pi^+\pi^-$ are dominated by $\Delta(1236)$ production, especially in the $|T_z| = \frac{3}{2}$ states. The $\Delta(1236)$ is present in nearly all the events. Double-isobar production of $\Delta^{++}(1236)$ and $\Delta^-(1236)$ accounts for about 24% of the reaction $p\bar{p} \rightarrow p\bar{p}\pi^+\pi^+\pi^-$. There is evidence for production of the $N^*(1525)$ in the reactions $p\bar{p} \rightarrow p\pi^+\pi^0 N^{*0}(1525)$, followed by $N^{*0}(1525) \rightarrow p\pi^-$, and $p\bar{p} \rightarrow p\pi^+\pi^- N^{*+}(1525)$, followed by $N^{*+}(1525) \rightarrow n\pi^+$.

D. Production of Meson Resonances

There is some evidence for production of the neutral meson resonances f^0 , η , and ω in reactions of the type $p\bar{p} \rightarrow p\bar{p} + (\text{meson resonance})$. The cross sections cor-

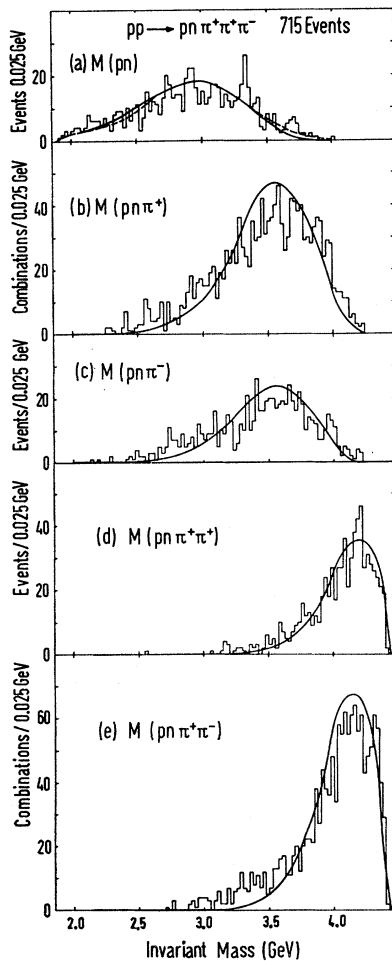


FIG. 21. Invariant-mass distributions for $p\bar{p} \rightarrow pn\pi^+\pi^+\pi^-$. (a) pn ; (b) $pn\pi^+$ (two combinations per event); (c) $pn\pi^-$; (d) $pn\pi^+\pi^+$; (e) $pn\pi^+\pi^-$ (two combinations per event). In (a) the dashed curve was calculated using diagrams 8–10 of Fig. 22.

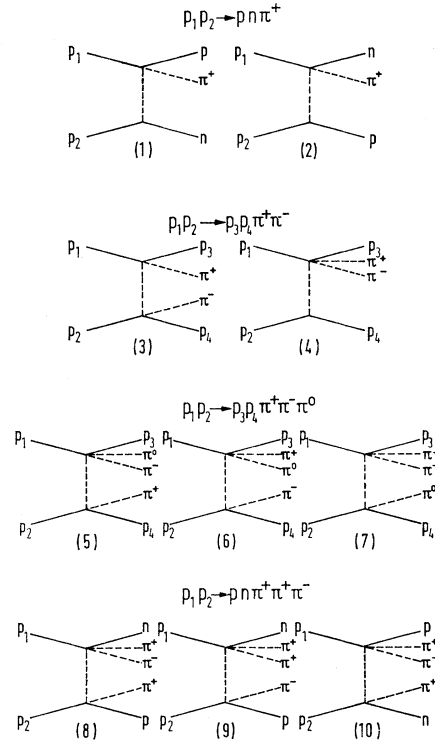


FIG. 22. OPEM graphs used in the Monte Carlo calculations.

rected for unobserved decay modes³⁸ are

$$\sigma(p\bar{p} \rightarrow p\bar{p}f^0) = 0.10 \pm 0.04 \text{ mb},$$

$$\sigma(p\bar{p} \rightarrow p\bar{p}\eta) = 0.16 \pm 0.07 \text{ mb},$$

and

$$\sigma(p\bar{p} \rightarrow p\bar{p}\omega) = 0.16 \pm 0.03 \text{ mb}.$$

The latter two are comparable with the values found in $p\bar{p}$ experiments at lower energies.^{1,3} The cross sections for production of these resonances are of the same order of magnitude as those found in $\pi p \rightarrow \pi p(f^0, \omega, \eta)$ at similar energies.⁴²

ACKNOWLEDGMENTS

We would like to express our gratitude to the operating crews of the CERN PS and Saclay bubble chamber, and the personnel of the computing facilities both in Cambridge and at DESY. We are especially grateful to Dr. E. Lohrmann for his personal interest in this work. Thanks are due to Dr. H. O. Wüster and Dr. D. Lublow of DESY for their help with computing problems. We also like to thank our scanning and measuring crews for their outstanding efforts. We are indebted to Dr. P. Söding, Dr. A. G. Forson, Dr. B. A. Westwood, Dr. A. Wolf de Benedetti, and Dr. G. Wolf for their advice and encouragement, and to R. Schäfer

⁴² C. Caso, G. Tomasini, P. Dittman, G. Drews, P. von Handel, H. Nagel, L. Mandelli, S. Ratti, V. Russo, G. Vegni, P. Daronian, A. Daudin, C. Kochowski, and C. Lewin, Nuovo Cimento 47A, 675 (1967).

and J. Höppner for valuable assistance in the analysis. The Hamburg group has been supported by the Bundesministerium für Wissenschaftliche Forschung. One of us (W. P. S.) thanks the Volkswagen Foundation for a fellowship.

APPENDIX A: MONTE CARLO ESTIMATE OF THE CONTAMINATION MATRICES

In order to get the true number of events in the different channels, the Monte Carlo program FAKE¹⁹ was used to investigate the sources of ambiguity. In this way criteria were developed to assist in accepting or rejecting hypotheses.

This program was used to generate bubble-chamber "events" taking into account the specifications of the chamber, range-energy loss, Coulomb scattering, and measurement errors. The strong forward-backward peaking of the nucleons (Fig. (1)) and the formation of the $\Delta(1236)$ resonance were also incorporated. These events were then processed through the same fitting programs (GRIND, etc.) that processed the real events. In analyzing the fits obtained it was assumed that pions could be distinguished from protons at laboratory momenta up to 1.7 GeV/c, the same momentum limit as was used for the bubble-density measurements in the actual events.

The elements of the normalized contamination matrices (W) for the fitted events are defined by

$$W_{IJ} = (\text{number of events generated by FAKE in channel } J \text{ that fit channel } I) / (\text{total number of events generated by FAKE in channel } J).$$

For the no-fit channels, the different possible "no-fits" were weighted using isotopic-spin considerations.⁴³

One gets the true number of events N_I in channel I for the actual experiment using the relation

$$N_I \pm \Delta N_I = \sum_J U_{IJ} F_J \pm (\sum_J F_J^2 \Delta U_{IJ}^2 + \sum_J U_{IJ}^2 \Delta F_J^2)^{1/2},$$

where F_J is the number of accepted hypotheses in channel J in the experiment and U_{IJ} are elements of the inverse matrix of (W). From

$$(U)(W) = (I)$$

we get

$$(\Delta U) = -(U)(\Delta W)(U).$$

The contamination matrices used for the two- and four-

⁴³ Y. Yeivin and A. de Shalit, *Nuovo Cimento*, **1**, 1146 (1955); V. S. Barašenkov and B. N. Barbašev, *Nuovo Cimento Suppl.* **7**, 19 (1958); S. Z. Belen'kij, V. M. Maksimenko, A. I. Nikisov, and I. L. Rozental, *Fortschr. Physik* **6**, 524 (1958); F. Cerulus, *Nuovo Cimento Suppl.* **15**, 402 (1960); J. Shapiro, *ibid.* **18**, 40 (1960), and references given therein. In πN collisions the distribution of various pion charge configurations follows a statistical isospin distribution rather closely. See, for example, K. Zalewski and J. A. Danysz, CERN Report No. TH 747, 1967 (unpublished), and references given therein; H. Satz [*Phys. Rev. Letters* **19**, 1453 (1967); **20** 238(E) (1968)] has used an additive quark model to connect multipion production in proton-proton and pion-proton collisions. His theory is in good agreement with our data.

prong events are given in Ref. 44. The number of ambiguous events A_{IJ} in channel I from channel J is simply $A_{IJ} = N_J W_{JI}$.

APPENDIX B: EVALUATION OF THE OPEM WITH FERRARI-SELLERI FORM FACTORS

The OPEM for the reactions $p p \rightarrow p n \pi^+$ and $p p \rightarrow p p \pi^+ \pi^-$ considers contributions of the diagrams 1 and 2 and diagrams 3 and 4 (Fig. 22), respectively, without interference.

The calculation of diagrams 1 and 2 is discussed in Ref. 10.

Diagrams 3 and 4 are called the "double-isobar" and "Drell" diagrams, respectively. They are calculated according to the form-factor OPEM by Ferrari and Selleri^{39,45-47} with experimental cross sections at the vertices. In their notation, we have the following matrix elements:

$$\text{diagram 3: } \sum |M_{fi}|^2 = \sum |M_+(\omega_1, \Delta^2)|^2 \frac{K'^2(\Delta^2)}{(\Delta^2 + \mu^2)^2} \times \sum |M_-(\omega_2, \Delta^2)|^2,$$

$$\text{diagram 4: } \sum |M_{fi}|^2 = \frac{\Delta^2}{4m^2} G_1^2 K^2(\Delta^2) \frac{K'^2(\Delta^2)}{(\Delta^2 + \mu^2)^2} \times \sum |M_0(\omega, \Delta^2)|^2.$$

Here \sum means summation over final- and averages over initial-particle spins; Δ^2 is the momentum transfer in the related diagram; m is the nucleon mass; ω_1 , ω_2 , and ω are the invariant masses of the vertex systems; $M_{\pm}(\omega_{1,2}, \Delta^2)$ is the matrix element for the reaction $\pi^{\pm} p \rightarrow \pi^{\pm} p$ and $M_0(\omega, \Delta^2)$ for $\pi^0 p \rightarrow p \pi^+ \pi^-$, with an incoming off-shell π ; $G_1^2 = 4\pi G^2(p p \pi^0)$; $G^2(p p \pi^0) = \frac{1}{2} \times 14.4$; and $K^2(\Delta^2)$ and $K'^2(\Delta^2)$ are form factors.

The off-shell matrix elements were determined from physical scattering processes by the relations

$$d\sigma_{\text{exp}}(\pi^{\pm} p \rightarrow \pi^{\pm} p) = \{\Lambda^2(\omega, \Delta^2) K^2(\Delta^2)\}^{-1} \times (2\pi)^{-2} \frac{m^2}{4F} \sum |M_{\pm}(\omega, \Delta^2)|^2 \delta^4(p_i - q_f) \frac{d^3 q_1 d^3 q_2}{q_{10} q_{20}},$$

$$d\sigma_{\text{exp}}(\pi^0 p \rightarrow p \pi^+ \pi^-) = \{\Lambda^2(\omega, \Delta^2) K^2(\Delta^2)\}^{-1} \times (2\pi)^{-5} \frac{m^2}{8F} \sum |M_0(\omega, \Delta^2)|^2 \delta^4(p_i - q_f) \frac{d^3 q_1 d^3 q_2 d^3 q_3}{q_{10} q_{20} q_{30}},$$

where $\Lambda^2(\omega, \Delta^2)$ is an off-shell correction.

⁴⁴ A. Schmitt, Diplomarbeit, Hamburg University, 1968 (unpublished); K. Strömer, Diplomarbeit, Hamburg University, 1967 (unpublished).

⁴⁵ E. Ferrari and F. Selleri, *Nuovo Cimento Suppl.* **24**, 453 (1962).

⁴⁶ E. Ferrari, *Nuovo Cimento* **30**, 240 (1963).

⁴⁷ E. Ferrari, S. Gennarini, and P. Lariccia, *Nuovo Cimento*, **39**, 169 (1965). A different form of the corrections was given by F. Selleri [*Nuovo Cimento* **40A**, 236 (1965)], but it leads to similar curves and to the same conclusions.

The unmeasurable cross section for $\pi^0 p \rightarrow p\pi^+\pi^-$ in diagram 4 was calculated in terms of the most recent data for $\pi^\pm p \rightarrow N\pi\pi$ using isotopic-spin arguments.⁴⁸

The combined form factors and off-shell corrections lead to the following expressions in the different diagrams:

$$\text{diagram 3: } A(\omega_1, \Delta^2)A(\omega_2, \Delta^2)G^{-2}(\Delta^2),$$

$$\text{diagram 4: } A(\omega, \Delta^2),$$

with

$$G^2(\Delta^2) = K^4(\Delta^2)K'^2(\Delta^2),$$

$$A(\omega, \Delta^2) = G^2(\Delta^2)\Lambda^2(\omega, \Delta^2).$$

In diagram 3, for $\omega \leq 1.45$ GeV we used

$$\Lambda^2(\omega, \Delta^2) = (q_{\text{off}}/q_{\text{on}})^2 \Gamma^2(\Delta^2) [1 + C(\omega, \Delta^2)]^2 G^2(\Delta^2),$$

where $G(\Delta^2)$, $\Gamma(\Delta^2)$, and $C(\omega, \Delta^2)$ are the same as in Ref. 39 and q_{off} (q_{on}) is the modulus of the three-momentum of an off- (on-) shell π in the c.m. system of a

⁴⁸ We have avoided using the approximate expression [Eq. (18) in Ref. 46] which neglects the sizable amplitude for isotopic spin $T(\pi\pi) = 2$. A detailed discussion of this point is given by J. H. Scharenguivel, Ph.D. thesis, Cambridge University, 1966 (unpublished).

πN state with an invariant mass ω . In all other cases we used

$$A(\omega, \Delta^2) = \left[1 + \frac{(\Delta^2 + \mu^2)}{\gamma} \right]^{-1}.$$

The additional diagrams obtained from diagrams 3 and 4 by interchanging initial or final-state protons are also included in the calculations neglecting all interference terms. Except where noted, the cutoff parameter [Eq. (4.10) of Ref. 39] was chosen to be $\gamma = 30 \mu^2$. This choice gave approximate agreement in the total cross section between the model and the experiment.

Distributions were calculated using a Monte Carlo program PHYSIK,⁴⁹ in which the complete kinematics of each generated event is available. Thus any desired selection criteria may be easily applied in order to compare the model with the corresponding experimental selection.

For the reactions $p\bar{p} \rightarrow p\bar{p}\pi^+\pi^-\pi^0$ and $p\bar{p} \rightarrow p\bar{p}\pi^+\pi^-\pi^-$, diagrams 5-7 and 8-10, respectively, were considered. Graphs with all the pions at the same vertex and interference between the diagrams were neglected.

⁴⁹ P. Söding (private communication). We used a modified version for the calculation of diagrams (5)-(10) of Fig. 22.

Measurement of the Branching Ratio and Positron Momentum Spectrum for the Decay $K^0 \rightarrow \pi^0 + e^+ + \nu$

D. R. BOTTERILL, R. M. BROWN,* A. B. CLEGG,† I. F. CORBETT, G. CULLIGAN, J. McL. EMMERSON, R. C. FIELD, J. GARVEY, P. B. JONES, N. MIDDLEMAS, D. NEWTON,* T. W. QUIRK, G. L. SALMON, P. STEINBERG,‡ AND W. S. C. WILLIAMS

Nuclear Physics Laboratory, Oxford, England

(Received 13 February 1968)

The branching ratio and positron momentum spectrum have been measured for the K_{e3}^+ decay mode. The shape of the momentum spectrum, containing 17 000 events, is consistent with pure vector coupling with a form-factor momentum dependence given by $\lambda^+ = 0.08 \pm 0.04$. Upper limits on a possible mixture of scalar or tensor coupling are, respectively, $|f_S/f_+| < 0.23$ and $|f_T/f_+| < 0.58$. The branching ratio is found to be $(4.92 \pm 0.21)\%$, based on 960 events. The semileptonic $\Delta I = \frac{1}{2}$ rule is tested by comparing the K_{e3}^+ and K_{e3}^0 rates. We conclude that the present data on K_{e3} decays are in disagreement with this rule.

WE assume that the matrix element¹ for K_{e3} decay is

$$M = [m_K f_S \bar{U}_\nu (1 + \gamma_5) U_e + \frac{1}{2} f_+ (p^K + p^\pi)_\alpha \bar{U}_\nu \gamma_\alpha (1 + \gamma_5) U_e + (1/m_K) f_T p_\alpha^K p_\beta^\pi \bar{U}_\nu \sigma_{\alpha\beta} (1 + \gamma_5) U_e],$$

where p^K and p^π are the four momenta of the K^+ and

π^0 , respectively. The form factors f_S , f_+ , and f_T for scalar, vector, and tensor coupling are functions of $q^2 = (p^K - p^\pi)^2$.² We assume that the q^2 dependence for vector coupling is given by the first two terms of a power-series expansion,

$$f_+(q^2) = f_+(0) (1 + \lambda^+ q^2/m_\pi^2).$$

The experiment was performed at the Rutherford High Energy Laboratory, using a 700-MeV/c separated

vector current should be written $\frac{1}{2}[f_+(p^K + p^\pi) + f_-(p^K - p^\pi)]$. The contribution from f_- however is proportional to m_e/m_K and has been neglected.

² The metric is chosen so that $q^2 = m_K^2 + m_\pi^2 - 2m_K E_\pi$, where E_π is the total energy of the pion.

* Now at the Rutherford High Energy Laboratory, Chilton, Berkshire, England.

† Now at the University of Lancaster, Lancaster, England.

‡ National Science Foundation Postdoctoral Fellow 1965-66, on sabbatical leave from the University of Maryland, College Park, Md.

¹ The factors m_K and $1/m_K$ are introduced to give f_S , f_+ , and f_T the same dimensions. The matrix element of the hadronic